FERROELECTRIC CERAMIC POLYMER NANO COMPOSITES FOR ELECTROCALORIC COOLING APPLICATIONS

A Thesis Submitted to
The Graduate School of Engineering and Science of
İzmir Institute of Technology
In Partial Fulfillment of the Requirements for the Degree of

MASTER OF SCIENCE

In Materials Science and Engineering

by
Melike TOKKAN

July 2020
İZMİR

ACKNOWLEDGEMENT

I would like to express my gratitude to my super advisor Dr. Umut Adem for his endless support during my study. Moreover, he always been the right person to lead me from an accurate guide in my study from an innovative perspective. In addition, I would like to thank Prof. Dr. Mustafa Muammer Demir for directing me to practical and rational solutions when I am in deadlock during my study. Thanks to them, I have acquired the knowledge and experience that I will use for a lifetime on this academic path that I have just entered.

I would like to thank Işın Özçelik, who carried out XRD analysis for my ceramic samples. I am also grateful to Ceren Aşkın, who performed XRD measurements of my film samples, and Prof. Dr. Ender Suvacı, who provided the opportunity to perform this analysis. I would like to express IZTECH Material Research Center where SEM analyzes are conducted, and Murat Delman, who conducted my FTIR analysis.

One of the most important thanks belongs to Assoc. Prof. Nandang Mufti, who enables us to take dielectric measurements in the shortest time possible with the developed Lab View program. I am also grateful to my dear friend Merve Karakaya, who developed this program and made it quick to get results.

The biggest thanks are to my dear mother Kevser Tokkan, my father Naci Tokkan, my sister Büşra Tokkan, who are always with me unconditionally, lift me whenever I fall, are behind me in every decision, who believe in my efforts whatever I do and what will I do, and do their best to motivate me.

One of the most important thanks belongs to my dear friends Merve Karakaya and Tuğçe Demirtay, whom I shared the same laboratory throughout my Master's life. We became lifelong friends who supported each other under all conditions. Moreover, I would like to express my gratitude to Barış Yıldırım, Remziye Yıldız, Sümeyra Sözer and Tuğçe Özmen Çulcular, who study in our neighboring laboratory, as they are all different sources of motivation. Finally, I would like to thank all my colleagues studying in research groups in the department of Materials Science and Engineering for being open and friendly in every respect.

ABSTRACT

FERROELECTRIC CERAMIC-POLYMER NANOCOMPOSİTES FOR ELECTROCALORIC COOLING APPLICATIONS

In this study, nanocomposites consisting of the polymer matrix and nanometer sized ceramic supporting phase were produced for electrocaloric cooling applications, which show potential as alternative refrigerant system. The aim of this study was to be able to estimate adiabatic temperature change (ΔT) of the composites by measuring saturated hysteresis loops for the composite materials that allow accurate calculation of the ΔT using the indirect method based on Maxwell's relations.

$Ba_{0.94}Ca_{0.06}Ti_{0.925}Sn_{0.075}O_3$(BCST) composition ceramic was used as the supporting phase of the composite and P(VDF-TrFE)(55-45) co-polymer was chosen as the matrix. The ceramics were synthesized, as pellets by conventional solid-state method. Ferroelectric nanocomposites were manufactured by solution casting method by adding 5, 7.5, 10 volume percent of the ceramic powder, which was obtained by grinding the pellets by using ball milling. Phase analysis of all materials done using X-ray Diffraction method. Fourier Transform Infrared Spectroscopy was used to clearly understand the phase structure of polymer. Scanning electron microscopy was used for understand the distribution of ceramic particles in polymer matrix. Dielectric constant-dielectric loss and ferroelectric hysteresis loops were measured as a function of temperature for the electrical characterization of the materials. Adiabatic temperature change under electric field (ΔT) of the materials were calculated based on Maxwell's equations indirectly using the temperature dependent electrical polarization data.

The dielectric constant and electrical polarization of the polymer matrix have increased with the addition of ceramic particles. The hysteresis loops of thebn pure polymer and composites were saturated, therefore the temperature change can be calculated accurately with the indirect method. Maximum ΔT was calculated on the composite having 10vol% ceramic particles. (6.964K at 900 kV/cm).

ÖZET

ELEKTROKALORİK SOĞUTUCU UYGULAMALARI İÇİN FERROELEKTRİK SERAMİK-POLİMER NANOKOMPOZİTLER

Bu çalışmada, alternatif bir soğutucu sistemi olabilecek potansiyele sahip olan elektrokalorik soğutucu uygulamalarına entegre edilebilecek, yüksek soğutma sıcaklığı etkisini sağlayabilecek nanometre boyutlu seramik destekleyici faz ve polimer matrisli kompozit malzemeler üretilmiştir. Bu çalışmanın amacı doyum noktasına ulaşmış ferroelektrik histerisiz davranışı gösteren ferroelektrik özelliklere sahip olan kompozit malzeme sentezlemek ve dolaylı yöntemle hesaplanan elektrokalorik sıcaklık değişimini seramik katkısı ile arttırmaktır.

Kompozit malzemenin destekleyici fazı $Ba_{0.94}Ca_{0.06}Ti_{0.925}Sn_{0.075}O_3$(BCST), matrisi ise Polivinilidienflorid-cotrifloroetilen P(VDF-TrFE)(55-45) olarak seçilmiştir. BCST, geleneksel katı hal yöntemi kullanılarak pelet halinde sentezlendikten sonra, saf P(VDF-TrFE)(55-45) polimeri, ve yüzde 5, 7,5, 10 hacim oranlarında seramik tozu (bilyalı değirmenle parçacık boyutu düşürülmüş) katkılanmış ferroelektrik polimer nanokompozitler çözeltiden döküm yöntemiyle sentezlenmiştir. Bütün malzemelerin faz analizleri X-ışını Kırınımı yöntemiyle yapılmıştır ve polimerin faz yapısını net olarak belirlemek için Fourier Dönüşümlü Kızılötesi Spektroskopisi kullanılmıştır. Seramik parçacıkların polimer matristeki dağılımı Taramalı Elektron Mikroskobu ile gözlemlenmiştir. Üretilen malzemelerin sıcaklığa bağlı olarak yapılan elektriksel karakterizasyonlarında, dielektrik sabiti ve ferroelektrik histerisiz eğrileri ölçülmüştür. Polarizasyonun sıcaklığa bağlı değişimi ve Maxwell's denklemleri kullanılarak malzemelerin adiyabatik sıcaklık değişimi değerleri hesaplanmıştır.

Katkılanma oranının artmasıyla polimer kompozitlerin dielektrik sabitleri ve elektriksel polarizasyon değerleri artmıştır. Polimer ve polimer-seramik filmlerin elektriksel polarizasyonu uygulanan elektrik alan ile doyum noktasına ulaşmıştır. Bu sayede, elektrokalorik sıcaklık değişimi değerleri (ΔT) doğruya yakın bir şekilde indirekt metotla hesaplanabilmiştir. En yüksek adiyabatik sıcaklık değişimi (ΔT) 900 kV/cm elektrik alan altında hacimce yüzde 10 seramik katkılanmış kompozit malzemede 6.96 (K) olarak elde edilmiştir.

TABLE OF CONTENTS

LIST OF FIGURES

Figure **Page**

Figure **Page**

Figure **Page**

Figure **Page**

LIST OF TABLES

Table **Page**

CHAPTER 1

INTRODUCTION

In this section, background information is given about ferroelectrics, electrocaloric effect and its applications.

1.1. Refrigerant Technologies and Their Problems

Vapor compression refrigerant systems are used in cooling technologies. However, these systems have some drawbacks, which are related with polluting the environment. This type of cooling technology consumes high amount of electricity and releases Green House gases to atmosphere. In order to decrease Green House gases (Chlorofluorocarbon) and global warming effect to the world, many countries signed the Kyoto Protocol. It has been agreed in the Kyoto Protocol to reduce the harmful gases emitted by the coolers working with the traditional vapor compression refrigerants. This leads the changes in trends towards alternative refrigerant technologies. There are many types of non-vapor compression based technologies, and the studies about non-vapor compression systems are increased. These cooling technologies are based on thermoelectric, magnetocaloric, electrocaloric and elastocaloric effects. The most common of them is the thermoelectric effect, but their low energy efficiency is barrier to replace vapor compression system. Caloric technologies utilize external electric field, mechanical force, and magnetic field to obtain temperature changes and are environmentally friendly. The caloric cooling based technologies have the potential to replace vapor compression based cooling technologies.[1] Electrocaloric cooling promising is a promising caloric cooling technology. The classes of ferroelectric materials, which have strong spontaneous polarization, show large electrocaloric cooling effect therefore we focused on these types of materials. In the following section ferroelectric materials are introduced.

1.2. Ferroelectricity Definition and the Brief History

Ferroelectricity is a certain property of materials, which exhibit reversible spontaneous polarization under external electric field.[2]

Rochelle Salt, which was the first material having ferroelectric properties, was discovered by Joseph Valasek. Before the ferroelectric properties were discovered, Potassium Hydrogen Tartrate ferroelectric material was found in the 1800s. David Bwester discovered the pyroelectric property (the spontaneous polarization as a function of temperature) of this material in 1824. In 1880, piezoelectric (showing stress changes under applied electric field) property of Rochelle Salt was understood by Jacques and Pierre Curie. In 1944, $BaTiO_3$, which is the member of the perovskite structure family, was produced and discovered ferroelectric properties. In 1952, Pb $(Zr,Ti)O_3$(PZT), which is the best known piezoelectric material, was discovered by G.Shirane and S.Hoshino.[3] The first ferroelectric polymer, PVDF (Polyvinylidene flouride), was discovered by Heiji Kawai in 1969.[4]

1.3. Ferroelectric Materials

Ferroelectric materials have polar crystal structure, which have positive and negative charge centers that do not overlap in the unit cell, these charges create the electric dipole moment, so the dipoles create the spontaneous polarization.[5] Ferroelectric, pyroelectric, piezoelectric, and dielectric properties of materials are interrelated; this relationship is shown in Figure 1.1. The classification of these properties based on symmetry is given Figure 1.2. Symmetry groups are divided into two subgroups, which are centro and non-centro symmetric. Piezoelectric materials have the basic non-centro symmetric crystal structure, and which also include polar symmetry. Pyroelectric materials have polar crystal structure. Ferroelectric materials have also polar crystal structure and additionally direction of their spontaneous polarization can be switched when the direction of electric field is reversed.[6]

In order to understand the switching mechanism of ferroelectric dipole moments, hysteresis loops, which shows the behavior of the material under applied electric field, should be examined. Figure 1.3 demonstrates a typical hysteresis loop of a ferroelectric material.[5]

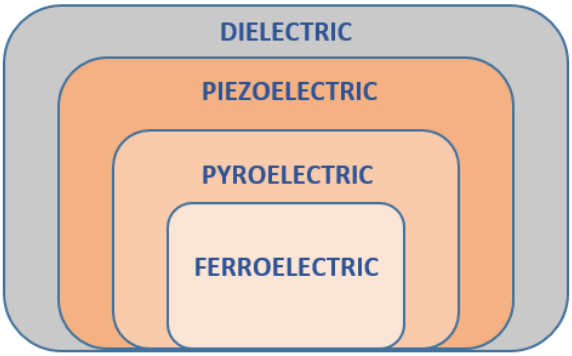

Figure 1.1.Schematic Illustration of the Relationship between Ferroelectrics, Pyroelectrics, Piezoelectrics and Dielectrics

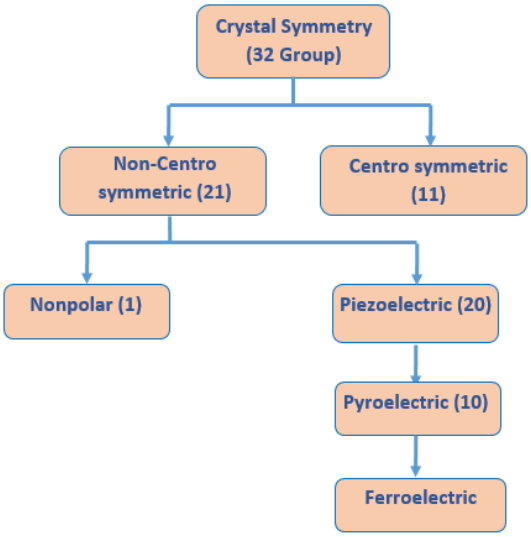

Figure 1. 2. Classification of the materials based on symmetry [5]

Firstly, the polarization ($\mu C/cm^2$) of the material increases linearly with the electric field applied to the material. The domains located in different directions with the throw of applied field, start to switch in the direction of the applied electric field and there is a nonlinear increase in polarization, because this mechanism occurs quite quickly. After all domains have been switched on, the polarization increase become linear again and the domains reach saturation point (P_s). When the applied electric field is reduced, some domains will be back switch. When the electric field value reached zero, the polarization value will not be zero. The polarization under zero electric field is determined remnant

polarization (P_r). To reduce polarization to zero, the direction of applied electric field must be changed. With the increase of the applied electric field to negative direction, the dipoles start to re-orient in the opposite direction and reach the saturation point again. Finally, the applied electric field decrease to zero point, and the loop cycle is reversed. The electric field value that makes the polarization value zero is called coercive field (E_C).[7] Figure 1.3 also shows that the formation of polarization mechanism is related to overlapping of Ti^{+4} ions of $BaTiO_3$ is from the center of the crystal symmetry due to non-centro symmetric behavior of $BaTiO_3$.

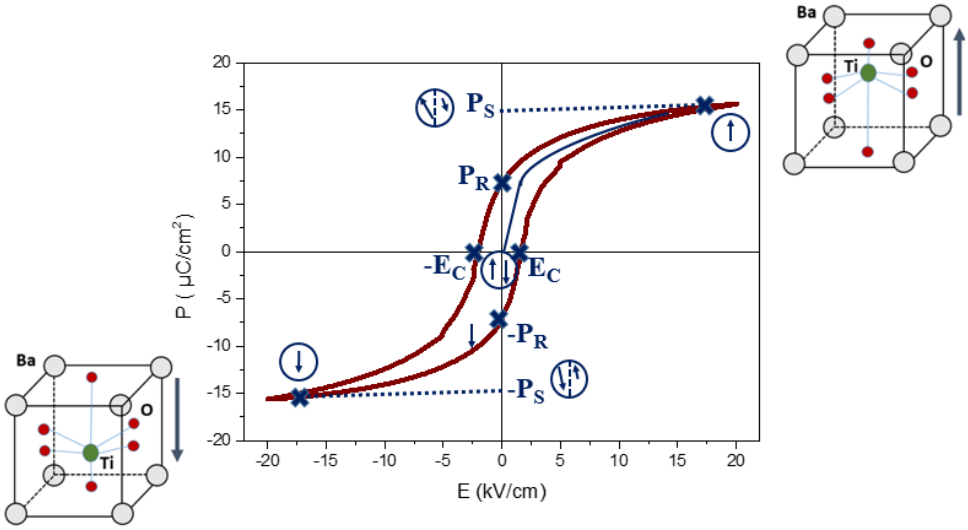

Figure 1. 3. Hysteresis Loop of a Ferroelectric Material

In addition to the hysteresis loops, a ferroelectric material has a critical temperature is called Curie temperature (T_C) showing the ferroelectric(non-centrosymmetric) paraelectric (centrosymmetric) phase transition.[7] This transition from the ferroelectric to paraelectric phase is the characteristics of the most ferroelectric materials, but there may be some exceptions. For example, in PVDF homo-polymer melting temperature is below the Curie temperature, therefore para-electric phase transition can't be observed this material.[8]

1.3.1. Relaxor Ferroelectricity vs. Normal Ferroelectricity

Relaxor material has some special polar nano regions (PNRs). PNRs, which is nanometer scale size (2-10nm), has spontaneous polarization different from nonpolar

regions. Nanodomains are formed with PNRs grows and connect to each other. The characteristic dielectric peak of relaxors is seen due to PNRs relaxation. Dielectric temperature of relaxors is defined T_m, and this is not similar to normal ferroelectric Curie temperature.[9] Figure 1.4 shows that dielectric, polarization versus temperature, and hysteresis loop behavior comparison of normal ferroelectric and relaxor feerroelectric materials.

The major contribution of dielectric constant is due to polar nano regions. The broad size of PNRs distribution and decreasing random interactions between PNRs causes widen distribution of relaxation time, and this brings about broadened dielectric constant versus temperature behavior. [10]

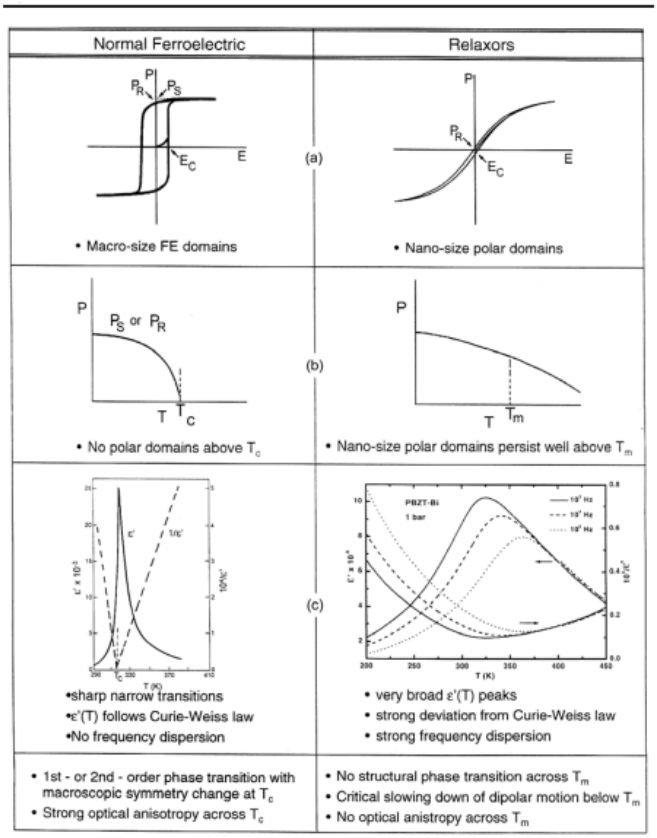

Figure 1. 4. The comparison of normal Ferroelectrics and Relaxor Ferroelectrics[11]

1.3.2. Ferroelectric Ceramics

There are different groups of ferroelectric ceramics; one of the important of them is perovskite-structured ceramics. The family members of perovskite ceramics are

$BaTiO_3$, PZT, PT (lead titanate), PLZT (lead lanthanum zirconate titanate) and $(Na,K)NbO_3$. Perovskites have ABO_3 type structure.[12]

Figure 1.5 shows that the crystal structure of $BaTiO_3$ (A site cation Ba, B site cation Ti) nonpolar phase (a), and polar phase (b) due to non-centrosymmetrical structure. According to this figure, $BaTiO_3$'s non-polar phase is cubic, polar phase is tetragonal. The ionic displacement causes the change of the crystal structure and spontaneous polarization under external electric field.[12]

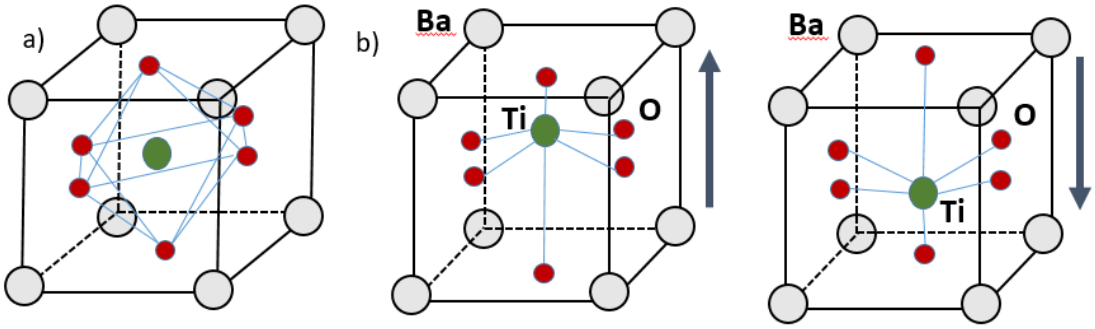

Figure 1.5. Position of atoms in perovskite structure (a) cubic (P_S=0), (b) tetragonal ($P_S \neq 0$)

$BaTiO_3$, a crucial ceramic of the perovskite ferroelectric material group, is a material with high dielectric constant and its Curie temperature is around 120ºC. The crystal structure of $BaTiO_3$ changes with temperature, and cubic, tetragonal, orthorhombic and rhombohedral phases are observed. The cubic phase of $BaTiO_3$ does not have ferroelectric properties, because Ti^{+4} is positioned at the center of mass of the oxygen octahedral. The phase transitions occur due to the distortion of TiO_6 octahedron with temperature.[12] Figure 1.6 shows that polymorphic phases of $BaTiO_3$ on the dielectric constant versus temperature graph. Temperature dependent polymorphic phases of $BaTiO_3$ are respectively: rhombohedral (T<-90ºC), orthorhombic (-90ºC<T<5ºC), tetragonal (5ºC<T<120ºC), cubic (T > 120ºC).[13]

One of the most important ferroelectric perovskite material, PZT (Lead Zirconate Titanate) is a ceramic and Zr^{+4} ions doped to Ti^{+4} B site: $PbZrO_3$-$PbTiO_3$. The PZT phase diagram shows the phases, as a function of temperature and composition (Figure 1.7.). Several phases can coexist in some special composition of this material, and this region is defined as MPB (morphotrophic phase boundary). PZT has a MPB in 52/48 ratio of Ti

/Zr at room temperature. MPB regions can show excellent properties, such as high piezoelectric constant and dielectric constant. In MPB region, six possible domain states in tetragonal phase <100>, 8 possible domain states in rhombohedral phase <111>, there are totally max 14 possible domain states. The total of all these domain states possibilities, which are coexisting around the MPB composition, provide the excellent ferroelectric, piezoelectric, pyroelectric properties. However, lead based materials are not environmental friendly.[12]

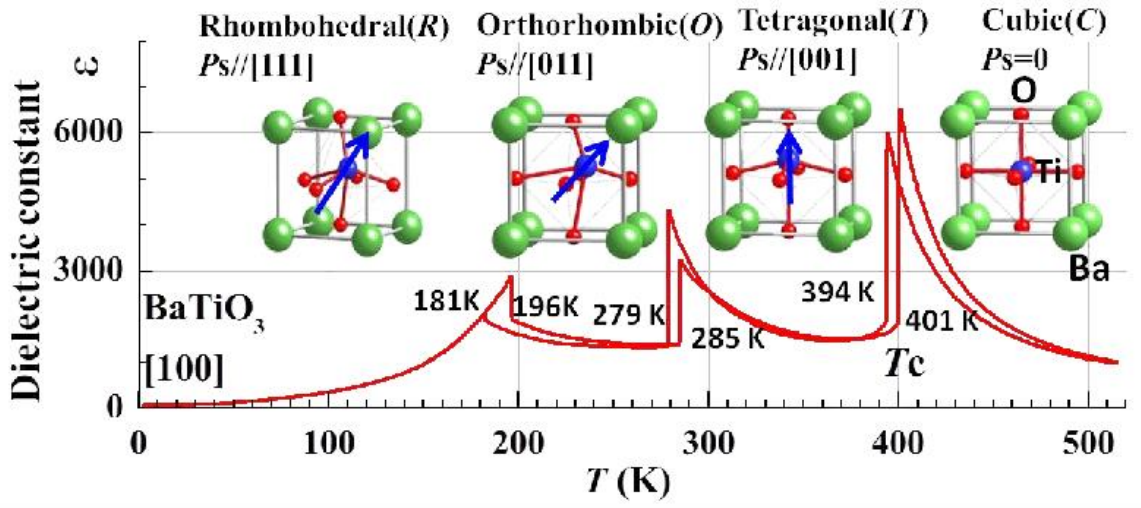

Figure 1. 6. Polymorphic phase transitions of $BaTiO_3$ on the Dielectric Constant versus Temperature Graph[13]

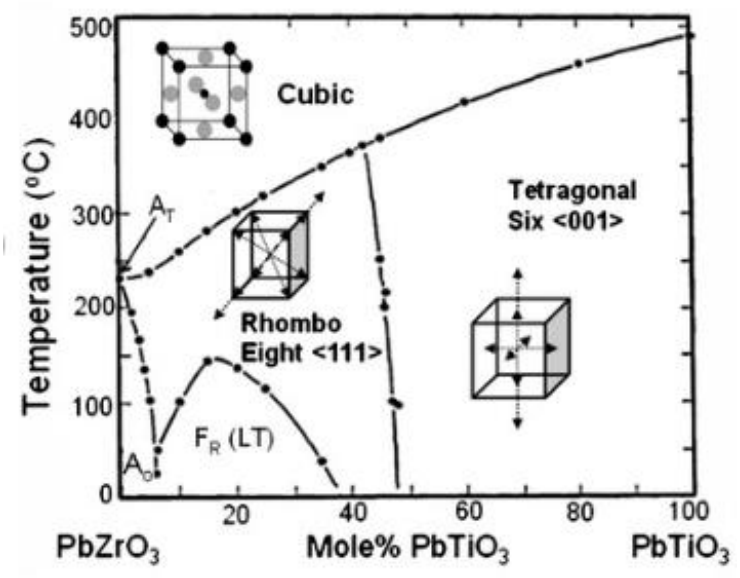

Figure 1. 7. Phase Diagram of PZT [14]

1.3.3. Ferroelectric Polymers

Polymers have generally insulating properties. Polymers are classified as polar and nonpolar polymers. Dipoles in the chain symmetries of non-polar polymers cancel out each other (no net dipole moment), so the dielectric constant values of such polymers are very low. Some examples of these polymers are PDMS (polydimethylsiloxane), PS (polystrene), LDPE (lowdensity polyethylene), PET (polyethyleneteraphlate), etc. In polar polymers, dipoles cannot dampen one another, so a net dipole moment occurs, thus the dielectric constants of polymers are higher. Chain geometry also contributes to the formation of polar structure in this type of polymers. Polarity arises from the difference of between the elements forming the bonds in the polymer change. The element having higher electronegativity creates a partial negative charge, having lower electronegativity creates a partial positive charge. The dipolar orientations of polymers are associated with the entanglement of long chains. [15]

PVDF is one of the most important polymers among polar polymers. A monomer of PVDF polymer is given Figure 1.8(a) PVDF, which is a semi crystalline polymer, can be transformed into more than one polymorphic phase. These phases are called Alpha (α), Beta (β) and Gama (γ). The chain entanglement of each phases are different from each other, Figure 1.8. (b), (c), (d) show the differences of chain entanglement among phases. The only polar phase of the PVDF is beta phase, which has thermodynamically stable spontaneous polarization, because this phase has TTT (all trans) chain entanglement. In this conformation, fluorine atoms are located in one region of the chain and hydrogen atoms are located in the other region. Fluorine atoms create partial negative charge due to high electronegativity, hydrogen atoms create partial positive charge due to lower electronegativity.[15] Various methods are applied to obtain the beta phase. These methods are poling, annealing at high temperature, drawing, stretching, annealing at high pressure, etc.[16]

In order to improve the polar structure of PVDF, the beta phase must be stable. Since it is very difficult to obtain 100% crystalline beta phase, copolymers, which have different two monomers, have been developed with various monomer addition to VDF monomer in the literature. When co-P(VDF-TrFE) is formed by connecting with VDF and TrFE monomers, conformation of TTT (all trans) is generated by attaching the bulk group TrFE to VDF chain (weakening intermolecular interaction).[16] Moreover, ıt causes

low alpha and gamma, high beta phase formation in copolymers that crystallize with has low content of TrFE under applied high electric field. Therefore, copolymer, which has low contents of TrFE, shows favorable ferroelectric and piezoelectric properties.[17] In addition, different types of copolymer are produced by adding HFP (hexafluoropropene) and CTFE (cholorotrifluoroethylene) monomers to VDF. The crystallinity of P(VDF-HFP) is lower than PVDF homopolymer, HFP increases the amorphous phase of crystal structure. The contribution of electrical properties associates with the addition rate and synthesis method. In addition to the copolymers, terpolymers, which consist of three different monomers, are also available. The one of the important of them is P(VDF-TrFE-CTFE). When synthesizing of P(VDF-TrFE) copolymer, the distance between chains allows another monomer to settle, so cholorofluoroethylene can settle this space, with the addition of this co-monomer the distance between the chains is reduced. The repeat parts of copolymer and terpolymer materials are given in Figure 1.9.

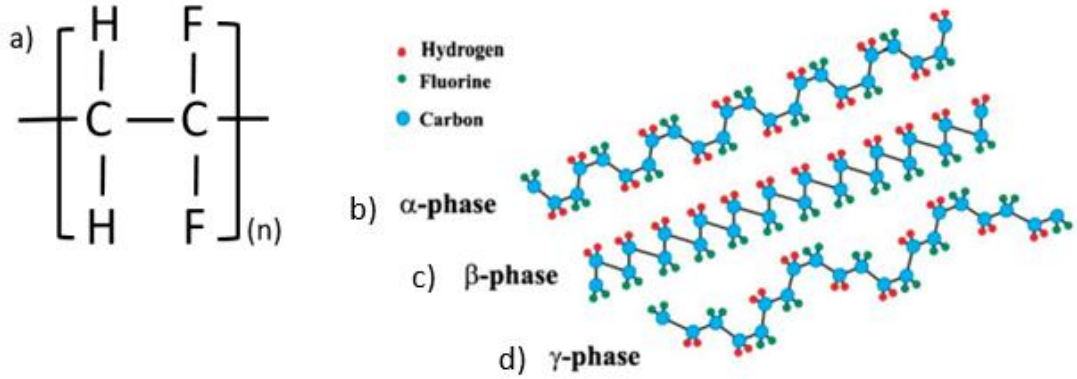

Figure 1. 8. (a) The chemical structure of PVDF monomer (b) ,(c) ,(d) The polymorphs chain conformation of PVDF[18]

In order to understand ferroelectric properties of PVDF based polymer, the hysteresis loop behavior of these types of polymer must be investigated. Figure 1.10 (a) demonstrates that the hysteresis loop behavior of alpha, beta and gamma phases of PVDF at 10Hz. As mentioned previously, the beta phase, which is only ferroelectric phase of PVDF, shows rectangular shaped hysteresis loop behavior, is normal ferroelectric with high remnant and maximum polarization. Displacement term can be used instead of polarization term in polymer systems, because the polarization values of polymer are lower than ceramics.[17] Figure 1.10 (b) demonstrates the hysteresis loop behavior of 55-

45 composition of P(VDF-TrFE) copolymer at 10 Hz. Similar to beta phase PVDF, P(VDF-TrFE) copolymer has also rectangular shape hysteresis loop, which shows the normal ferroelectric behavior.

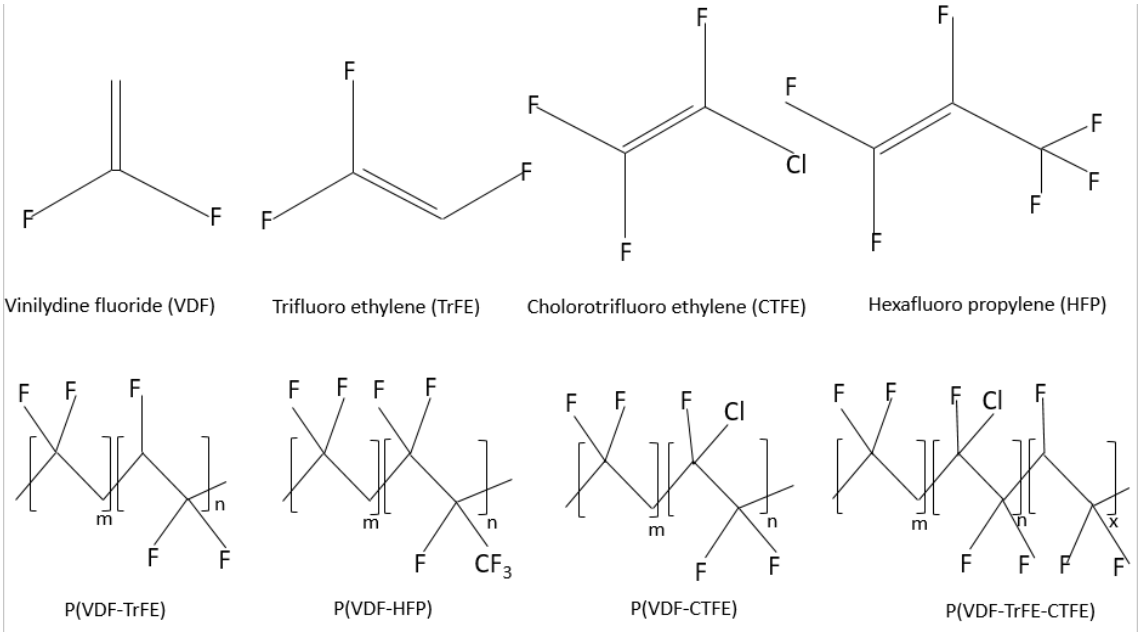

Figure 1. 9. Schematic illustration of (VDF), (TrFE), (HFP) and (CTFE) monomers and P(VDF-TrFE), P(VDF-HFP),P(VDF-CTFE) and P(VDF-TrFE-CTFE) repeat units[19]

In the Figure 1.9, the individual monomers, co-monomers, ter-monomers, which are found in PVDF based copolymer and terpolymer, are shown. Co-monomers insertion of PVDF chains increases the formation of ferroelectric effect with a steric blocking effect. For example, when P(VDF-co-TrFE) is formed, inserting an extra fluorine atom ensures that the chain entanglement under T_C all trans (TTTT) (where the TrFE concentration is more than 11%). The presence of the $–CF_3$ group P(VDF-co-HFP) copolymer provide dipole orientation easily. P(VDF-CTFE), like other copolymers, has an effect that ensures piezoelectric constant and ferroelectric properties developing. Creating PVDF copolymers reduces the activation energy required for the phase transition from alpha phase to beta phase by increasing the distance between chains, regardless of processing method. When third monomer is added to P(VDF-TrFE) copolymer, the chain conformation changes from TTTT to TGTG or T_3G. In addition, termonomer reduces the domain size and causes wide ferroelectric paraelectric phase

transition (Curie temperature decreases close to room temperature). These reasons show reduction of ferroelectric behavior in terpolymer. Therefore, terpolymers of PVDF is classified under ferroelectric relaxors.[17] The comparison of the electrical properties of these most commonly used homo polymer, copolymer and terpolymer are given Table1.1. The changes of interchain distance with comonomer and third monomer addition to PVDF chain is shown at Figure 1.11. Moreover, this figure demonstrates the appearance of the nanodomains and relaxor behavior in PVDF based terpolymer and irradiated copolymer because of the increase in the interchain spacing hysteresis loops of relaxor based PVDF terpolymer and irradiated copolymer are also given the figure 1.11.

Table 1.1. Comparison of the electrical properties of beta phase of PVDF, P(VDF-TrFE), P(VDF-HFP), P(VDF-TrFE-CTFE) [15, 19-23]

POLYMER	MELT. TEMP (°C)	DIELECTRIC CONSTANT (ε_r)	LOSS TANGENT	MAX. POLARIZATION ($\mu C/cm^2$)	d_{33} ($pC.N^{-1}$)
PVDF	~170[20]	6-12[15]	0.025[15]	6.5[15] (1500 kV/cm)	24-34[19]
P(VDF-TrFE) (55/45)	~158[20]	18[21]	<0.1[21]	8 [21] (1500 kV/cm)	25-40[19]
P(VDF-HFP)	~140[20]	11[15]	0.4[15]	7[15] (5500 kV/cm)	24[19]
P(VDF-CTFE) (91/9)	165 [20]	13[15]	0.03[15]	8[22] (6000 kV/cm)	140[19]
P(VDF-TrFE-CTFE) (80/12/2%mol)	120-140	47 [15]	0.21[15]	5.2 (3000 kV/cm)	81.64[23]

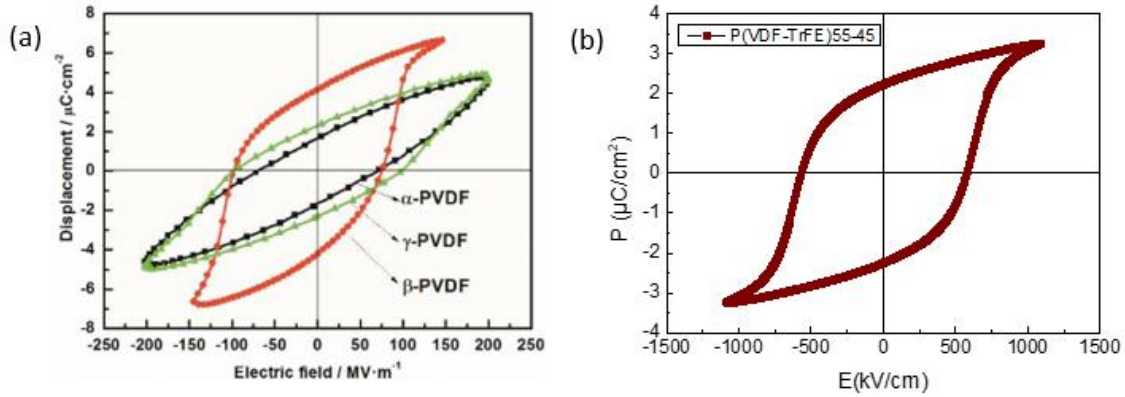

Figure 1.10. (a) The hysteresis loop behavior of alpha, beta and gamma phase of PVDF[17] (b) the hysteresis loop behavior of P(VDF-TrFE) 55-45

1.3.4. Ferroelectric Composites

Composites are a group of materials produced by combining two or more classes of materials with different phase structures. Ferroelectric composites can exhibit improved functional properties, which are needed by modern electronic devices. Each part of composite might contribute particular properties. For example, a composite material consisting of ceramics, which have high piezoelectric constant with high breakdown strength with polymer matrix, can be used for an actuator, which is highly desired.[24] Ferroelectric composites are generally combined with ceramic-ceramic, polymer-ceramic, polymer-polymer materials group. Composites, which have polymer matrix (primary phase) and ceramic supporting phase (secondary phase and stronger than matrix), are group of materials that can be alternative for ferroelectric applications.[25-27]

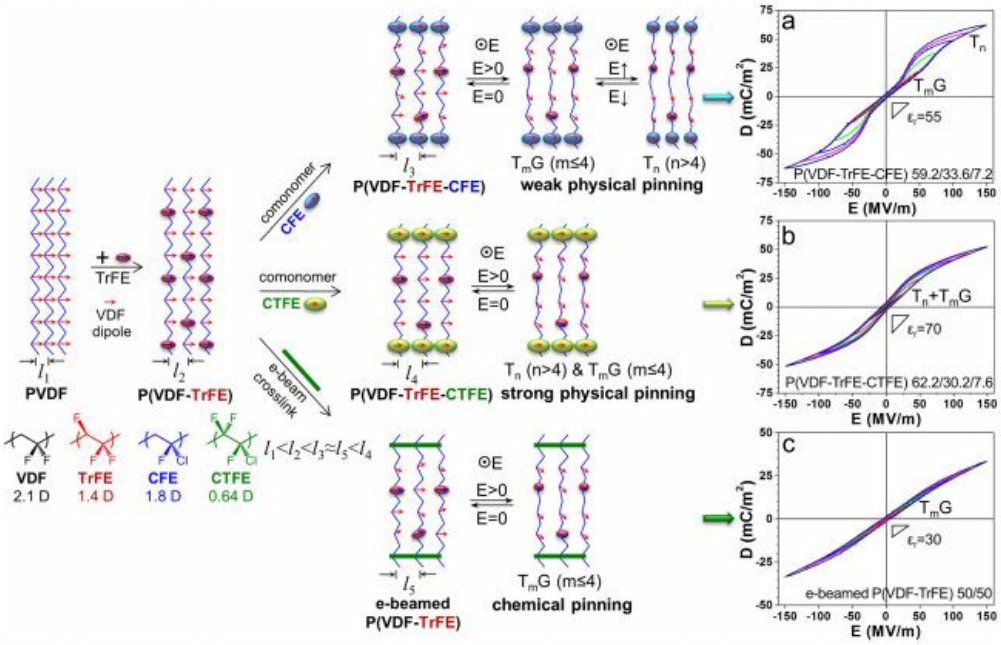

Figure 1.11. The change of interchain distance with the addition of co and third monomer to PVDF homo-polymer, and the effects of interchain distance on the ferroelectric properties[22]

One of most important factors in the formation of composites is that the phases used should be wetting each other very well; it means that the phases should stick together. Matrix and reinforcement are connected in different forms. The connectivity relationships of two-phase systems are shown Figure 1.12. In two phase systems; 0-0, 0-

1, 0-2, 0-3, 1-1, 1-2, 1-3, 2-2, 2-3, 3-3 connectivity types are available (these connectivity and numbers are introduced by Newnham[28]). The most preferred type is 0-3 type (first number shows the active phase second number shows the inactive phase, number 3 means that there is 3 dimensional connection), where reinforcement phase is randomly distributed in the matrix phase. For two phases of composites, two dimensional connection can be found between the phases, therefore the composites, which have 2-2 connectivity, show the properties of laminar types of composites. [29]

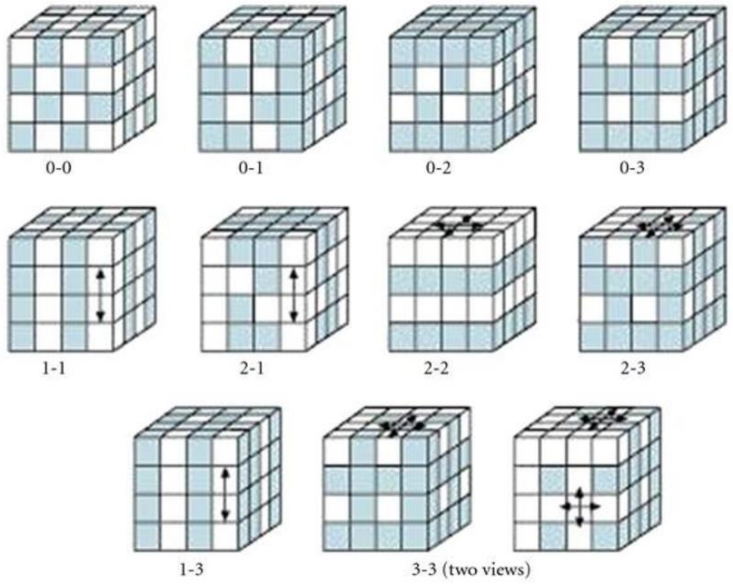

Figure 1. 12. Generally used connectivity types of two phase composite [30]

1.3.4.1. Applications of Ferroelectric Composites

There are different types of applications of polymer ceramic composite systems for different demands. Ferroelectric polymer ceramic composites are used in capacitor, transducer and actuator applications.[31]

Energy storage devices (capacitors) should have large breakdown strength and dielectric constant. Materials, which have higher dielectric constant, give higher polarization at lower electric fields, and perovskite ceramics has higher dielectric constant. Breakdown field or dielectric strength is defined as the endurance of materials to high external electric field without failure. Polar polymers have long chains, and they need high amount of electric field for polarizing these chains. Breakdown strength of the

polymers is higher than those of the ceramics. Capacitive energy storage is calculated by using equation1.1. According to this equation, highest amount of maximum polarization and electric field is necessary for higher discharge efficiency, the production of composite materials provide both of the properties.[32]

$$U_e = \int_{P_R}^{P_m} EdP \qquad (1.1.)$$

Polymer ceramic composites are also used in piezoelectric applications. The working principle of transducers is related to the converse piezoelectric effect. The working principle of actuators associate with direct piezoelectric effect. The most common connectivity types of the composites are 2-2(laminar form of fillers), 1-3(fiber form of fillers) for piezoelectric applications, because the longitudinal direction of fillers is parallel to polarization direction in these types of connectivity. Perovskite ceramic materials have high piezoelectric charge constant (d_{33}), most well known ferroelectric perovskite is PZT, however lead based piezoelectric ceramics are not environmental friendly. Polymers have high dielectric breakdown and mechanical strength for the piezoelectric applications. Composites that consisted of piezoelectric ceramic and polymer might bring good properties of both materials. The different piezoelectric applications are energy harvesting system, actuator, transducer, biological device, MEMs (micro electromechanical systems), etc. According to demands of applications, the characteristics of composites can be modified.[33]

1.4. Electrocaloric Effect

In this section, the definition, history, measurement methods, potential applications of the electrocaloric effect and electrocaloric materials that can be used for applications will be discussed.

1.4.1. Definition and History

Electrocaloric effect, which is a physical phenomenon, refers to fact that the materials with dipolar constituents become ordered or disordered with an externally

applied electric field (under adiabatic conditions), and temperature changes obtained with the changes in the subsystem entropies of the dipoles. [34]

Electrocaloric effect was first determined theoretically as an inverse effect of pyroelectricity by William Thomson. In 1943, Kobenkov and Kurshatov calculated the first adiabatic temperature change of Rochelle Salt (0.003K). In 1962, it was determined that maximum elecrocaloric effect properties where found at the Curie temperature. After these developments, efforts have been made to increase electrocaloric temperature and entropy change in many organics and inorganics, so research is ongoing to make them available.[35]

Figure 1.13 demonstrates the changes in the states of dipoles under applied electric field. When an electric is applied to a dielectric material whose dipoles are randomly distributed, the dipoles became oriented. Since the ambient conditions are adiabatic, the total entropy does not change, while the dipolar entropy decreases, lattice vibration entropy increases, so temperature increases. The electric field is removed when the dipoles turn to random state. The dipolar entropy increases while the vibrational entropy decreases, therefore temperature decreases.[34]

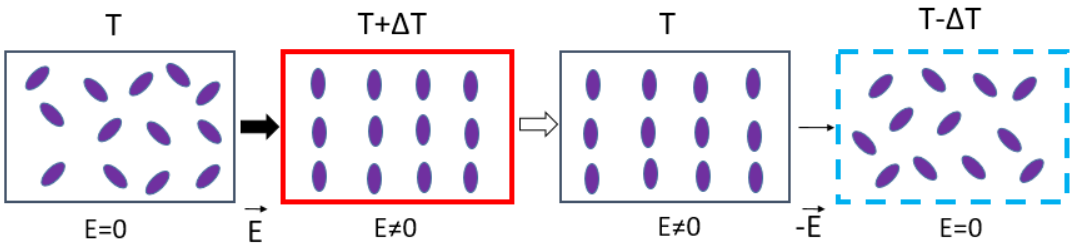

Figure 1.13. Schematic illustration of ordering and disordering of electrical dipoles with the applied electric field in a electrocaloric cooling cycle (modified from[34])

Electrocaloric systems, which create cooling effect of materials having ferroelectric dipoles under applied electric field, without using any gas and pressure can be compared to conventional compressors used today. In Figure 1.14, the cooling cycles of both systems are given. In the adiabatic environment, temperature increases by compressing of the gas with pressure in the conventional compressors and by the formation of isothermal polarization (dipoles orient, so dipole entropy reduces and lattice entropy therefore temperature increases) of dipoles in elecrocaloric coolers. In the reverse situation, temperature decreases by expansion of gas with reduced pressure in

conventional compressors and, by reducing of the lattice vibration entropy and increasing of dipole entropy in the electrocaloric coolers.[34]

1.4.2. Measurements Method of ECE

The electrocaloric effect is measured directly and indirectly.

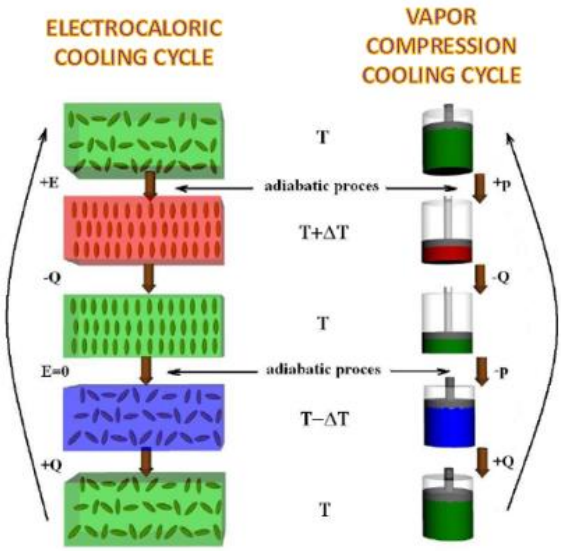

Figure 1.14. Schematic Illustration of the Electrocaloric and conventional Vapor Compression based Cooling Cycle [36]

1.4.2.1. Indirect Method

Indirect method is based on the calculation of the electrocaloric temperature change and using Maxwell's equations and by using the information obtained from the temperature dependent ferroelectric hysteresis loops. The equation 1.2 is derived from the differential form of Gibbs free energy and isothermal entropy and adiabatic temperature change are calculated by using equation 1.3 and 1.4.

$$\left(\frac{\partial S}{\partial E_i}\right)_T = \left(\frac{\partial P_i}{\partial T}\right)_E \tag{1.2}$$

$$\Delta S = -\frac{1}{\rho}\int_{E_1}^{E_2}\left(\frac{\partial P}{\partial T}\right)_E dE \tag{1.3}$$

$$\Delta T = -\frac{T}{C_P * \rho}\int_{E_1}^{E_2}\left(\frac{\partial P}{\partial T}\right)_E dE \tag{1.4}$$

In this equation, T is the temperature, (ρ) is the density, (E) is the electric field, (C_P) is specific heat capacity under constant electric field, adiabatic temperature change (ΔT), isothermal entropy change (ΔS), differential change of polarization as a function of temperature under constant electric field ($(\partial P/\partial T)_E$). In order to calculate ΔS and ΔT, it is necessary to obtain $(\partial P/\partial T)_E$. P(T) is extracted from temperature dependent hysteresis loops. According to these values, P(T) curve can be drawn and a polynomial can be used to fit the curve and by differentiating the fitted curve $(\partial P/\partial T)_E$ can be obtained. Alternatively without performing the fit, $(\partial P/\partial T)_E$ can also be calculated by using equation 1.5.[37]

$$\left(\frac{\partial P}{\partial T}\right)_E = \frac{1}{2} * \left(\frac{P_n - P_{n-1}}{T_n - T_{n-1}} + \frac{P_{n+1} - P_n}{T_{n+1} - T_n}\right) \tag{1.5}$$

In the electrocaloric effect studies, indirect measurement is preferred(%85) because it is giving faster results and it is relatively easy to conduct. Direct methods have also some drawbacks. [38-42] Indirect measurements also have some drawbacks, such as inapplicability for relaxor ferroelectrics.

1.4.2.2. Direct Method

Direct measurement systems calculate the adiabatic temperature change in the material from the applied electric field by means of measuring either heat flux or temperature without any extra calculations. Figure 1.15 shows the calorimeter and thermal sensors used for direct method respectively; (a) DSC (b) heat flux sensor and thermocouples (c)thermistors (d)infrared thermal sensors and cameras. DSC (Differential Scanning Calorimetry) devices can measure EC heat flux in under applied electric field.

From the values of heat flux the entropy and temperature changes can be calculated. In order to measure changes of adiabatic temperature change by using DSC, various modifications are needed.[34]

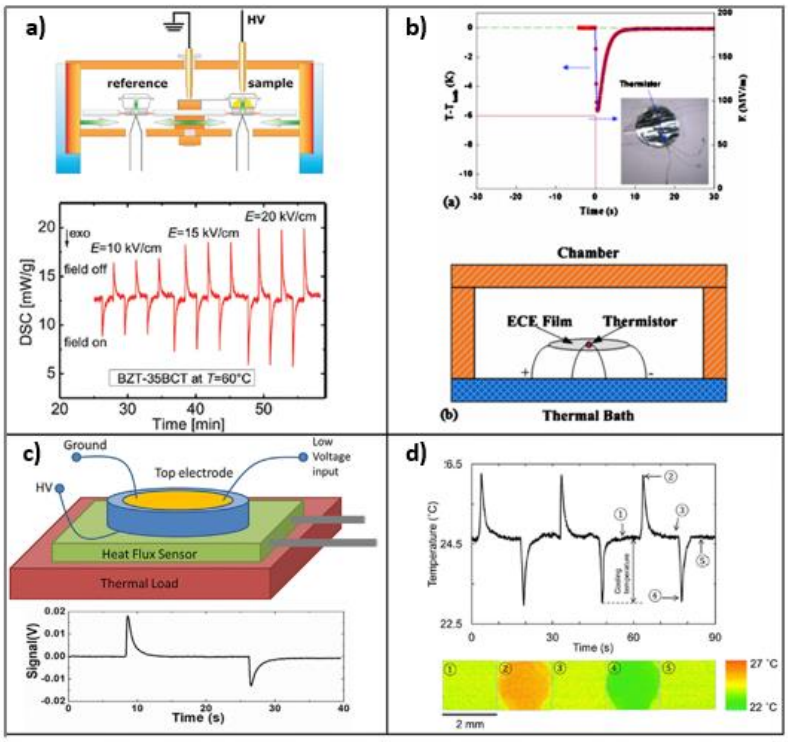

Figure 1.15. The schematic representations of direct measurements of electrocaloric effect using (a) DSC, (b)heat flux and sensors, (c) thermistors and (d) infrared temperature sensors and camera[1]

Direct measurements have some drawbacks, due to these drawbacks, in general indirect measurements (depend on Maxwell's equation) are preferable for the electrocaloric effect studies, but however for some types of materials, indirect measurements cannot be used if accuracy is needeeds. For example, relaxor ferroelectrics are not in thermal and mechanical equilibrium, because they have polar nanodomains which have regions that act as ferroelectric but are not ferroelectric.[37]

1.4.3. Electrocaloric Materials

In order to obtain a high ECE according to Landau Devonshire theory and Maxwell's equations, the materials must show high polarization change as a function of

temperature change. Ferroelectric materials can achieve this in the ferroelectric (FE) paraelectric (PE) phase transition region, because the domains will be random above Curie temperature, so the polarization of the material drops. It is important that EC materials can provide adiabatic temperature change close to room temperature. Relaxor ferroelectrics, which have polar nanoregions, have high polarization values under a small electric field, because their nanodomains can be oriented under small electric fields. They show a high ECE in a wide temperature range (close to room temperature), however their ECE can be measured accurately only with the direct method.[1]

Organic and inorganic FEs or relaxor FEs are produced as a single crystal or polycrystalline bulk, thick film and thin film forms.[1] Some of organic, inorganic and composite based ECE studies are compared in table 1.2 in terms of ECE properties. Electrocaloric strength is defined as the adiabatic temperature change divided by electric field ($\Delta T/ \Delta E$). Generally, the electrocaloric strength (K.m/MV) values of ceramics are higher than the other groups, because low amount of electric field is enough the make that their ferroelectric domains aligned. However, the dielectric breakdown strength of ferroelectric ceramics is low. ΔT values and breakdown strength of the polymers are generally higher than ceramics, but their electrocaloric strength values are lower. Because they have long chains, and the orientation of the dipole moments of polymers in long chain needs high amount of electric field. Therefore, in order to improve ECE performance, many research groups tried composite materials, which have ceramic filler and polymer matrix parts. Their results show the enhancement of ECE with ceramic filler addition to the polymer matrix.[43-45] Relaxor terpolymer and their composites enhance the ECE properties most, but direct methods must be used for the calculation of their ECE due to their thermodynamically unstable nanodomains.

1.4.4. Potential Applications of Electrocaloric Cooling Technology

Conventional cooling systems (air conditioners, refrigerators, etc.) use the harmful gases such as HFC (hydrofluorocarbon) which leads to the global warming. It is predicted that the direct emission of these harmful gases will constitute 45% of the CO_2 emission in 2050. The refrigerants used today contribute to the global warming indirectly. Cooling systems also have high share in the electricity consumption in the many countries (America: 22%, China: 14%). It is considered that electrocaloric coolers can potentially

meet the need of environmentally friendly cooling technologies, especially in terms of carbon emission and Green House effect.[1]

Table 1. 2. Summary of electrocaloric properties of different types of materials

Material	Form	T(ºC)	ΔE (kV/cm)	ΔT(K)	ΔS (J/kgK)	Method	Reference
$Ba_{0.65}Sr_{0.35}TiO_3$ +Mn	Bulk	20	90	3.08	4.77	Indirect	Liu et.al.[46]
$BaTiO_3$	Thick Film	80	800	7.1	10.1	Direct	Bai et.al.[47]
$BaZr_{0.2}Ti_{0.8}O_3$	Thick Film	40	97	4.9	8.536	Direct	Hui Jian et.al.[48]
$BaTiO_3$	Single Crystal	97-147	10	1.6	1.9	Direct	Bai et.al.[49]
$Ba_{0.995}Ce_{0.005}Ti_{0.99}Mn_{0.01O3}$	Bulk	120	30	1.22	-	Indirect	Liu et. al.[50]
$0.92(Na_{0.5}Bi_{0.49}Nd_{0.01}TiO_3) – 0.08(BaTiO_3)$	Bulk	67-87	50	0.95	-	Indirect	Kandula et.al.[51]
$PbZr_{0.95}Ti_{0.05}O_3$	Thin Film	226	480	12	-	Indirect	Mischenko et. al.[38]
$(PbMg_{1/3}Nb_{2/3}O_3)0.7 - (PbTiO_3)0.3$	Bulk	145	90	2.6	-	Direct	Rožič et.al. [52]
$Pb_{0.8}$ $Ba_{0.2}ZrO_3$	Thin Film	135	598	45.3	46.9	Indirect	Peng et.al. [53]
P(VDF-TrFE) 55/45	Thick Film	80	2090	12.6	62	Indirect	Neese et.al. [41]
P(VDF-TrFE-CFE) 59.2/33.6/7.2	Thin Film	30	1500	14.8	73.5	Direct	Li et.al.[54]
P(VDF-TrFE) 68/32	Thin Film	33	1600	20	95	Direct	Lu et.al.[55]
P(VDF-TrFE-CFE) 62.5/29/8.5 – P(VDF-TrFE)55/45	Thin Film	20-60	750	5	-	Direct	Chen et.al. [56]
P(VDF-TrFE-CFE)-BST67	Thin Film	30	2500	50.5	210	Direct	Zhang et.al. [57]
P(VDF-TrFE-CFE)-PMN/PT	Thin Film	30	1800	31	150	Direct	Li et.al. [43]
P(VDF-TrFE)52/48-$Ba_{0.75}$ $Sr_{0.25}TiO_3$	Thin Film	75-80	600	2.5	-	Indirect	Jiang et.al. [45]

Figure 1.16 demonstrates the published articles about ECE in the last twenty years. The studies of ECE increased every year, and this shows the demand for environmentally friendly cooling systems. In addition, the prototypes of electrocaloric coolers is developing together with the number of studies on ECE. Some examples of EC prototypes, will be examined in this section.

Zhang, Z. et al. designed a cooling device by using P(VDF-TrFE-CFE) polymer. Device consists of CNT(single walled carbon nanotubes electrode) conductive layer frame coated on thick PET film due to electrostatic actuation. EC terpolymer was stacked on PDMS. Their device is attached to Li-ion battery, and they attached a thermocouple for to measured temperature changes. In air, temperature of the battery has decreased 3ºC

in 50 seconds. When they tried cooling by using EC device, the temperature of battery have decreased 8ºC in 5s at 6.77MV/m electric field at 0.8 Hz.[58] This demonstrates that EC cooling device can help as microcooling device..

Gu. et al. designed a circle-like refrigerant system where hot and cold plates are located mutually, unlike the potential other cooling devices designs. The schematic representation and working principle of this system is shown in Figure1.17 (They obtained ΔT:0.86K under 200 V for Y5V ceramic composition).[59] In addition, Zhang, Q. et.al. synthesized BST nanowire-BNN-P(VDF-TrFE-CFE) composite and obtained a cooling power density of 400W/cm^3.[60]

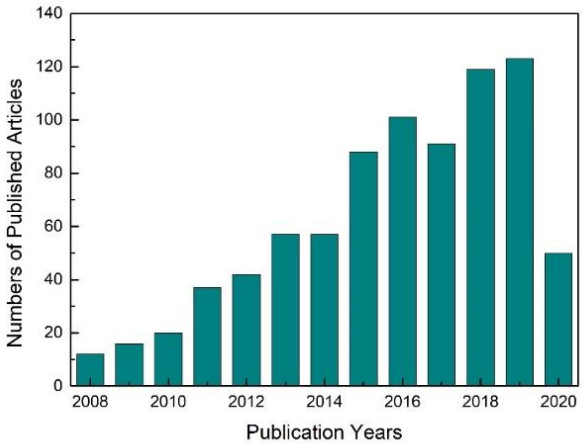

Figure 1. 16. The number of published articles with the topic 'electrocaloric' in the last 12 years (Web of science search with the topic electrocaloric, on June 22th,2020)

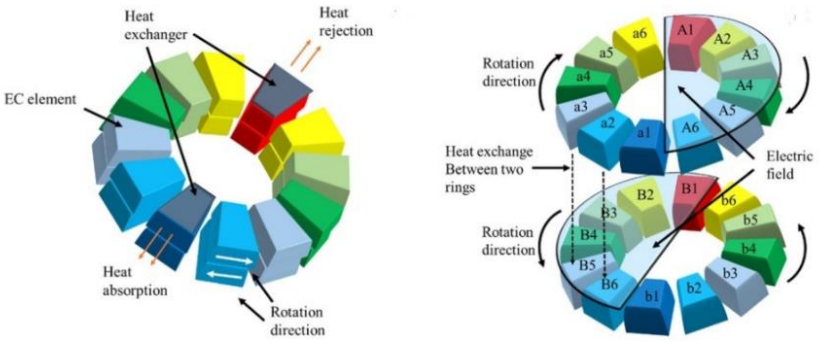

Figure 1.17. The schematic illustration of designed potential cooling device by Zhang, Q. et.al. and working principle of device[59]

1.5. Literature Review

The studies about polymer ceramic based composite systems using electrocaloric cooling applications increases day by day. In this section, some of the electrocaloric effect studies on polymer ceramic composite systems will be explained.

Jiang et.al. synthesized a composite using solution casting method by combining the BST supporting phase (10%volume, 26% mass ratio) with 30 nm particle size synthesized with the hydrothermal method and P(VDF-TrFE)52/48 polymer as the matrix phase. It was emphasized that the Curie temperatures of the composite phases should be close to each other because the max ΔT value at ECE is obtained in the Curie temperature region. If matrix and filler parts Curie temperature values are very different from each other, the max ECE could not be observed, because both of them create max ECE at different temperature area. They used the indirect methods for ECE calculations. They observed that the ΔT value of composites was higher than pristine polymer. They suggested that increase is caused by the local dielectric and ferroelectric properties occurring in areas close to ceramic and polymer interface. Comparison of the hysteresis loops of the composite and pristine copolymer at room temperature (a) and polarization versus temperature attitude of composite (b) are show in Figure 1.18. The polarization value of pristine copolymer is lower than that of BST-P(VDF-TrFE), the loops of both of them are not saturated. They obtain ΔT= 2.5 under 600 kV/cm.[45]

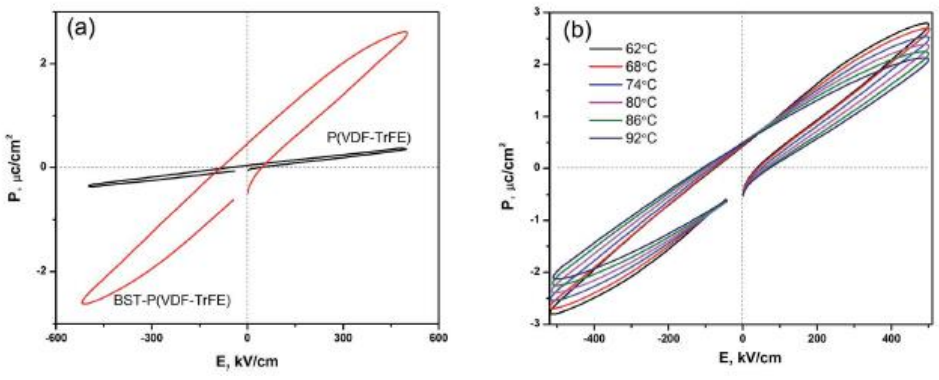

Figure 1.18. Temperature dependent P(E) loops for (a) Pristine P(VDF-TrFE) and BST-P(VDF-TrFE), (b)BST-P(VDF-TrFE) [45]

Aziguli et al. synthesized composite consisting of P(VDF-TrFE-CFE) 61.3/30.5/8.2 (relaxor) polymer matrix and addition of 0, 2.5, 5, 7.5, 10% volume ratio

$BaZr_{0.2}Ti_{0.8}$ O_3 ceramic reinforcement parts. The reinforcement part produced with conventional solid state methods, and particle diameter was 1 µm. Composites were synthesized by solution casting method and N,N-Dimethylformamide used as polar solvent, and direct method with specially designed calorimeter was used for the measurement of ECE properties. They obtained maximum ΔT= 7.4 K and ΔS= 30 J/kgK under 900 kV/cm at around 25ºC for (5vol %) BZT-P(VDF-TrFE-CFE) composite. The ΔT value was found almost 1.5 times larger than that of pristine terpolymer. This result shows that the addition of ceramic filler increases ECE performance, but ΔT value decreased with above the 5vol% concentration of the ceramic. Figure 1.19 shows Q, ΔT, ΔS values.[61]

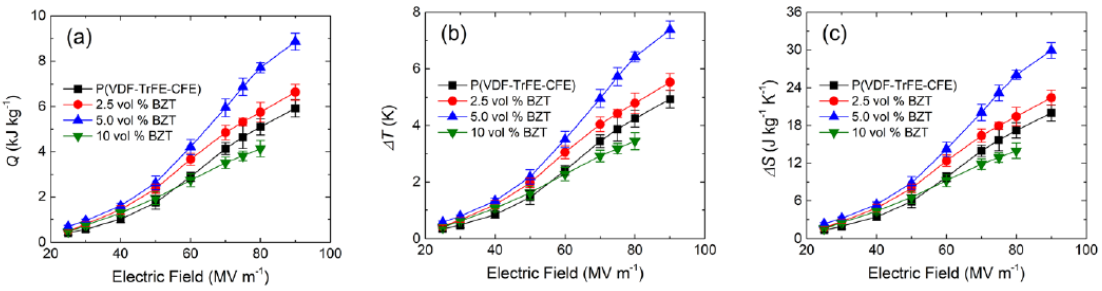

Figure 1.19. Q(a), ΔT(b), ΔS(c) comparison of P(VDF-TrFE-CFE) terpolymer and BZT-P(VDF-TrFE-CFE) composites at room temperature and different electric field[61]

Li et.al synthesized composites consisting of P(VDF-TrFE-CFE) 59.4/33.4/7.2 relaxor terpolymer (produced with suspension radical polymerization) and $0.9Pb(Mg_{1/3}Nb_{2/3})O_3$- $0.1PbTiO_3$ relaxor ceramics as the reinforcement phase. Addition of 37.5 wt% filler content provide maximum ECE properties ΔT= 9.4K ΔS=85 kJ/Mk at 750 kV/cm. ECE of 37.5 weight percent of ceramic filler added composites was better than pristine polymer, and only 75 V was enough for EC cooling. The dielectric displacement of the composites increased with the filler addition. Above the 37.5 wt% filler addition to the polymer matrix decreases the ECE. Changes of crystallinity and interfacial coupling factor, which are affected by the volume fraction at interfacial layer, changed the adiabatic temperature change. Both volume fraction and crystallinity degree were maximum for the composition, which has of 37.5wt% filler, so it showed the best ECE performance. ΔT and ΔS graphs are given in Figure 1.20.[43]

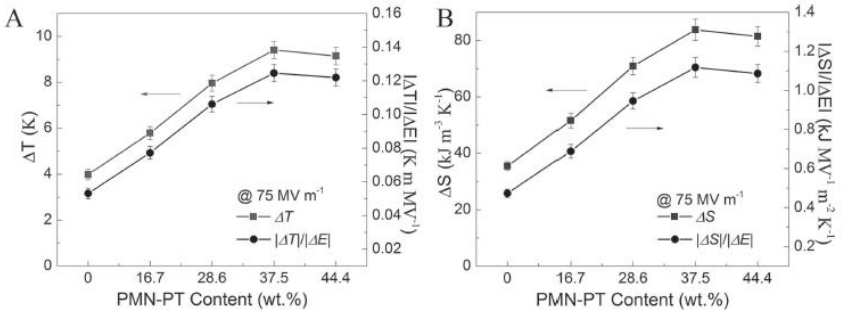

Figure 1. 20. PMN-PT-P(VDF-TrFE-CFE) composites (a) ΔT, (b) ΔS values at the different filler addition under 750 kV/cm electric field[43]

Zhang et al. synthesized the BST ($Ba_{0.67}Sr_{0.33}TiO_3$) reinforce P(VDF-TrFE-CFE) (62.3/29.9/7.8) matrix nanocomposite. BST produced in the form of nanoparticle (average diameter: 180nm), nanowire (average diameter: 120nm), nanocube (average diameter: 200nm) and nanorods (average diameter: 300nm) with hydrothermal method. They manufactured the nanocomposite with DMF solvent by solution casting. Addition of the filler phase in different morphology caused different results in terms of electrical properties. The highest aspect ratio was found the BST nanowire. The dielectric constant of %15 BST nanowire added composites was 72.5; this was higher than other morphologies. In this study, composite materials, which have high ECE properties, were produced by Zhang et.al. Figure 1.21 shows that the ECE properties (ΔT, ΔS, and Q (T* ΔS)) of nanocomposites with 10 vol% nanofiller and pristine terpolymer at 1000 kV/cm all morphologies of nanofiller BST increases the ECE properties.[44]

In general ceramic filler addition to polymer matrix improves the ECE properties. There are some explanations about the enhancement mechanism of ECE. One of them is interfacial coupling There is an interface between ceramic and polymer parts of composites. Ferroelectric ceramics have the strong dipole moment, and they do not need high electric field, however polymer, which has long chain configuration), needs high electric field for their ordering of their dipole moment. Ceramics, which are polarized at lower electric field will amplify the applied electric field and increase the effective electric field acting on the polymer matrix increasing the electrical polarization. In addition, new dipole moments might from in the interface close to ceramic filler region causing interfacial. Some research groups proven that the interface effect between ceramic particles and polymer matrix region by using Piezoresponse Force Microscopy.

[62] Optimal filler addition to polymer matrix is important for enhancement of electrocaloric effect. Above a critical concentration called the percolation concentration, fillers are too close to each other and are aggregated. Inside the filler, electric field increases too much, this causes harder orientation of dipole moments inside the filler. Therefore, polarization changes dependent on temperature decreases.[63] In addition, shape, formation, size of filler is very important for EC composite systems. Fillers should distribute homogenously in composites for obtaining good electrical properties. If it is not distributed homogenously, this leads to voids or defect like behavior in systems, and this effect the properties of composites.[44]

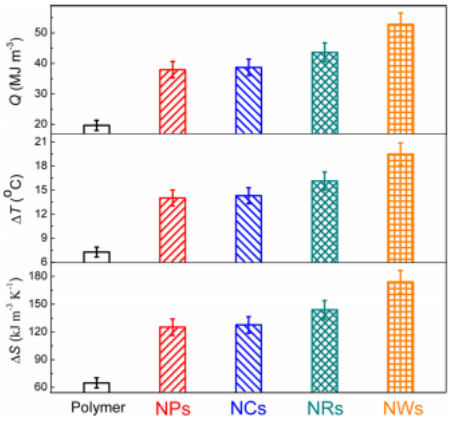

Figure 1.21.Q, ΔT, ΔS values comparison of P(VDF-TrFE-CFE) polymer and 10%BST(Np, Nc, Nr,Nw)-P(VDF-TrFE-CFE) nanocomposites at 1000 kV/cm[44]

1.6. Research Objectives

In this study, nanocomposites, which have P(VDF-TrFE) 55/45 polymer matrix and $Ba_{0.94}Ca_{0.06}Ti_{1-x}Sn_xO_3$ ceramic reinforcement particles were studied. One of the purposes of this study is the development of ECE performance with filler addition into the polymer matrix. To obtain saturated hysteresis loop for composite materials is the second aim of this study. Since indirect measurement methods are used, the hysteresis loops of nanocomposites must be saturated and exhibit ferroelectric properties. In addition, it was necessary to choose Curie temperature ranges of the filler and matrix phase close to each other, because maximum adiabatic temperature change is obtained at the Curie temperature. In electrocaloric cooling systems, it is desirable that the cooling

effect is as close to room temperature as possible, therefore Curie temperatures must also be close to the room temperature.

PVDF can used as the matrix material, but only the beta phase is polar phase and obtain to a hundred percent of beta phase requires extra processing. Also the Curie temperature of PVDF (195ºC) is higher than melting temperature (177ºC), so it cannot be used for ECE applications. Therefore, when the other copolymers are examined, P (VDF-TrFE) copolymer, which have high dielectric constant and polarization value, was chosen. When the phase diagrams of the P(VDF-TrFE) copolymer in the literature are examined, the 55/45 composition, showing the normal ferroelectric(not relaxor ferroelectric) property with the Curie temperature closest to room temperature, was chosen. The Curie temperature of 55/45 composition is ~68ºC.

As a reinforcement phase, it has been found suitable to choose $BaTiO_3$, one of the environmentally friendly lead free ferroelectrics. The Curie temperature of $BaTiO_3$ is around 120ºC. As stated above, the Curie temperatures of the phases of nanocomposites should be close to each other, and to achieve that Ca (A site) and Sn (B site) doped to $BaTiO_3$ decrease the T_C. Wang et al. studied Ca and Sn doped $BaTiO_3$.[64] The composition of BCST ($(Ba_{0.94}Ca_{0.06})(Ti_{0.925}Sn_{0.075})O_3$), which has similar Curie temperature with P(VDF-TrFE) 55/45 was chosen based on Wang. et al.'s results.

The main aim of this study is to obtain a high ΔT value under a moderate electric field that can be used in electrocaloric cooler applications with thick film composites produced with solution casting method. Addition ceramic filler to polymer matrix improves electrocaloric cooling performance performance of the materials according to previous studies. It was aimed to investigate using indirect measurements.

CHAPTER 2

EXPERIMENTAL

2.1. Sample Preparation

Experimental steps are given separately for:

a) Synthesis and characterization of $(Ba_{0.94}Ca_{0.06})(Ti_{0.925}Sn_{0.075})O_3$ ceramic nanoparticles.
b) Synthesis and characterization of pristine P(VDF-TrFE) (55/45) polymer thick film.
c) Synthesis and characterization of the composite materials by the addition of 5, 7.5 and 10 volume percent of ceramic nanoparticles into polymer matrix.

2.1.1. Synthesis of $(Ba_{0.94}Ca_{0.06})(Ti_{0.925}Sn_{0.075})O_3$

The production flow chart of the ceramic part of the composite material given in Figure 2.1. Conventional solid-state method was used for the manufacturing of the reinforcement part of the composites. Before the composites were synthesized, the ceramics were produced in pellet form and characterized.

To synthesize the $(Ba_{0.94}Ca_{0.06})(Ti_{0.925}Sn_{0.075})O_3$ ceramic, $BaCO_3$ (99.9% Entekno), TiO_2 (99.9% Sigma Aldrich), $CaCO_3$ (99.999% Sigma Aldrich) and SnO_2 (99.9% Merck) starting powders were kept at 200ºC overnight in the thermal oven (Memmert UF55). The starting powders were stoichiometrically weighed on the analytical balance (RADWAG- AS220. R2) and mixed with ethanol and Yttrium stabilized Zirconia balls (diameter: 5 mm) in 30 ml HDPE Nalgene bottle. After the mixture was mixed in the Planetary Ball Mill (RETSCH PM 100) for 250 rpm 8 hours, ethanol is evaporated from powder at 70ºC in the thermal oven. Then the mixture of powders was calcined at 1200ºC for 4 hours in high temperature furnace (Protherm Muffle Furnace). The powders were mixed again at 250 rpm for 8 hours in planetary ball mill and solvent evaporated. PVA (Polyvinyl alcohol) that was used for binder and 2 % weight of powders were dissolved pure water at 80ºC and 250 rpm on magnetic stirrer

(Heidolph Hei-Tec). PVA solution and ceramic powders were mixed at same condition in the planetary ball mill, and solution was dried again. The powders were pressed with a Hydraulic Press (Specac) by applying 375 MPa pressure, thus the ceramic pellets, each weighing approximately 0.5 g, are obtained. Then the binder was burned out at 600ºC for 4 hours (1ºC/min ramp rate). Following the burn out process, ceramic pellets were sintered at 1350ºC for 3 hours. After sintering, the ceramic pellets were polished with SiC sand papers of 1000 and 2000 mesh for the electrical measurements.

2.1.2. Synthesis of Pristine P(VDF-TrFE) (55/45)

The flow chart for the synthesis of pristine polymer (0% ceramic doped) is given Figure 2.2. Solution casting method was used for the manufacturing of the polymer matrix. Before the composites are synthesized, the polymers were produced in thick film form and characterized.

To synthesize the pristine copolymer thick film, P (VDF-TrFE) 55/45 (PolyK Technologies) powders were dissolved in N,N-Dimethlyformamide (DMF) (5%wt). Then the solution was mixed at 500 rpm for 4 hours on the magnetic stirrer (Heidolph Hei-Tec) and sonicated for half an hour in the ultrasonic bath (ISOLAB), and then the solution was casted into the petri dish. DMF was evaporated at 70ºC overnight. To obtain the predominantly ferroelectric phase of the copolymer, heat treatment was applied at 135ºC for 3 hours (2ºC/min ramp rate). The final copolymer thick film was divided into small pieces for the characterization steps.

2.1.3. Synthesis of the Composites

The production flow chart of the composite (5, 7.5, 10 volume percent ceramic doped) is given Figure 2.3. Solution casting method was used for the production of thick film composite materials, similar to the pristine copolymer.

To synthesize the P (VDF-TrFE) 55/45- BCST composite, firstly BCST ceramic pellets were ground in agate mortar to obtain powder of BCST. Ball milling process was applied to reduce the particle size of the BCST powders. P(VDF-TrFE)55/45 copolymer, nanosized BCST powder, and DMF were weighed (5%wt). The copolymer powders were dissolved with DMF via the magnetic stirrer at 500 rpm for 4 hours. Then BCST ceramic

powders were added to the solution and the solution was mixed at 500 rpm for overnight. The solution was sonicated for half an hour in the ultrasonic bath and casted into the petri dish. DMF was evaporated at 70ºC, and heat treatment was applied at 135ºC for 3 hours (2ºC/min ramp rate). The thick film composites were divided into small pieces for the characterization steps by using scissors.

2.2. Materials Characterization

The characterization methods used for the synthesized are detailed in this section.

2.2.1. Density Measurements

The density determination kit of the RADWAG- AS220. R2 analytical balance was used for calculate the density of the BCST ceramic pellet materials. This density determination kit working principle is based on Archimedes' Principle.

According to the Archimedes' principle, the buoyancy force of an object immersed in a water or any liquid is equal to the weight of the liquid in which the object is displaced. Therefore, this principle is well suited for calculating the density of solid objects using the mass of solid objects in air and its effective mass in the water. The effective mass under water plus the mass of displaced water gives the actual mass of solid object. The amount of displaced fluid allows the volume of solid object to be calculated thus the density to be calculated. The formula used to calculate the density of ceramic pellets is given below. The symbols in the formula mean ρ: density, X: weight of the sample in air, Y: weight of the sample in the liquid, ρ_l: density of the liquid, ρ0: density of air.[65]

$$\rho = \frac{\mathrm{X}}{(\mathrm{X}-\mathrm{Y})}(\rho l - \rho 0) + \rho 0 \qquad (2.1.)$$

2.2.2. X-Ray Diffraction (XRD)

X-Ray Diffraction experiments were used to determine the crystal structures and phases of the synthesized materials. X Ray Diffraction experiments (Philips X'pert Pro)

were done at IZTECH Center for Material Research. XRD patterns of BCST are collected between 20º-80º angle range with 0.04 º/s scanning speed. X-ray diffraction measurements of thick film samples were done by using a Bruker D2 Phaser in Eskişehir Technical University (Ender Suvacı Laboratory). XRD patterns were collected using 0.02º/s scanning speed between 10-90º.

2.2.3. Scanning Electron Microscopy (SEM)

In order to get information about the microstructures of the samples, the analysis was carried out on scanning electron microscope(Philips XL 305 FEG and FEI Quanta 250 FEG in IZTECH Center for Materials Research). For BCST ceramic, polymer and composites, both backscattering and secondary electron detector images were recorded at different magnifications.

Etching process must be applied in order to distinguish grain structure and grain boundaries of polycrystalline ceramic pellet samples. The ceramic samples were kept in acetone solution for 1 hour before the thermal etching. The thermal etching process was performed by applying heat treatment for 1 hour at 100ºC below the sintering temperature. After thermal etching process, the ceramic pellets were waited again in the acetone solution. The polymer and composite films do not require any preliminary preparation. To obtain thickness of the thick films, the films were broken with liquid nitrogen. In the first time, thick films were cut with scissors, but this caused bending of the film. The bending causes problems in determining the thickness of the films and that's why generally the films were broken after freezing with liquid nitrogen.[66-68] Thick film samples were kept for ten seconds in liquid nitrogen, and samples could be broken easily. The ceramic, polymer and composite materials, which are insulators, were coated with gold by a sputter coating.

2.2.4. Fourier- Transform Infrared Spectroscopy (FTIR)

FTIR measures the vibration frequencies of various bonds and determines the functional groups in the molecules. In order to have an idea about the phase structures of polymer based materials, generally this method is used for supporting XRD experiment. ATR (Attenuated total reflectance) FTIR measurements were done with Perkin Elmer

Spectrum Version 104.3 in IZTECH Biotechnology and Bioengineering Application and Research Center. For the measurement, wavelength range was selected between 400-4000 cm^{-1} and transmittance (%) signals were measured.

2.2.5. Differential Scanning Calorimetry (DSC)

Differential Scanning Calorimetry (DSC) instrument measures the change the amount of energy in the sample under heating, cooling or at constant temperature. In addition, this instrument is used to determine thermal parameters such as specific heat capacity, phase transition temperature, reaction and conversion kinetics, degree of crystallinity of the materials. DSC measurements were used to get an idea about curie and melting temperature of synthesized samples in this study. TA Instruments Q10 was used at IZTECH Geothermal Energy Research and Application Center. The temperature range and heating rate were selected between 0°C and 200°C and 10°C/min, and the experiment was done under flowing nitrogen gas.

2.2.6. Dynamic Light Scattering Analysis (DLS)

Dynamic Light Scattering Analysis (DLS) is a spectroscopic method that examines the size distributions of small particles in a dilute suspension or solution. In this method, the light created by the monochromatic light source coming from the laser hits the particles in the colloidal suspension with Brownian motion which depends on the particle size, viscosity and temperature, then scattered light which is defined as Rayleigh scattering have different wavelength and intensities.[69] The formation of constructive and destructive interferencne due to Brownian motion between particles dispersed in the solution causes fluctuations in the intensity of scattered light. The change caused by these fluctuations in scattered light give cumulative information about the size distribution of the particles.[70]

Ceramic particles need to be as small as nanosize in order to disperse more easily and homogeneously in the polymer ceramic composites. Therefore, the sintered BCST ceramic pellets crushed using ball, 5 mg of ceramic powder was dispersed ultrasonically with 1.5 ml of ethanol. DLS measurements were done with Zetasizer NanoZS, Malvern Instruments at IZTECH Materials Science and Engineering Department (DemirLab.).

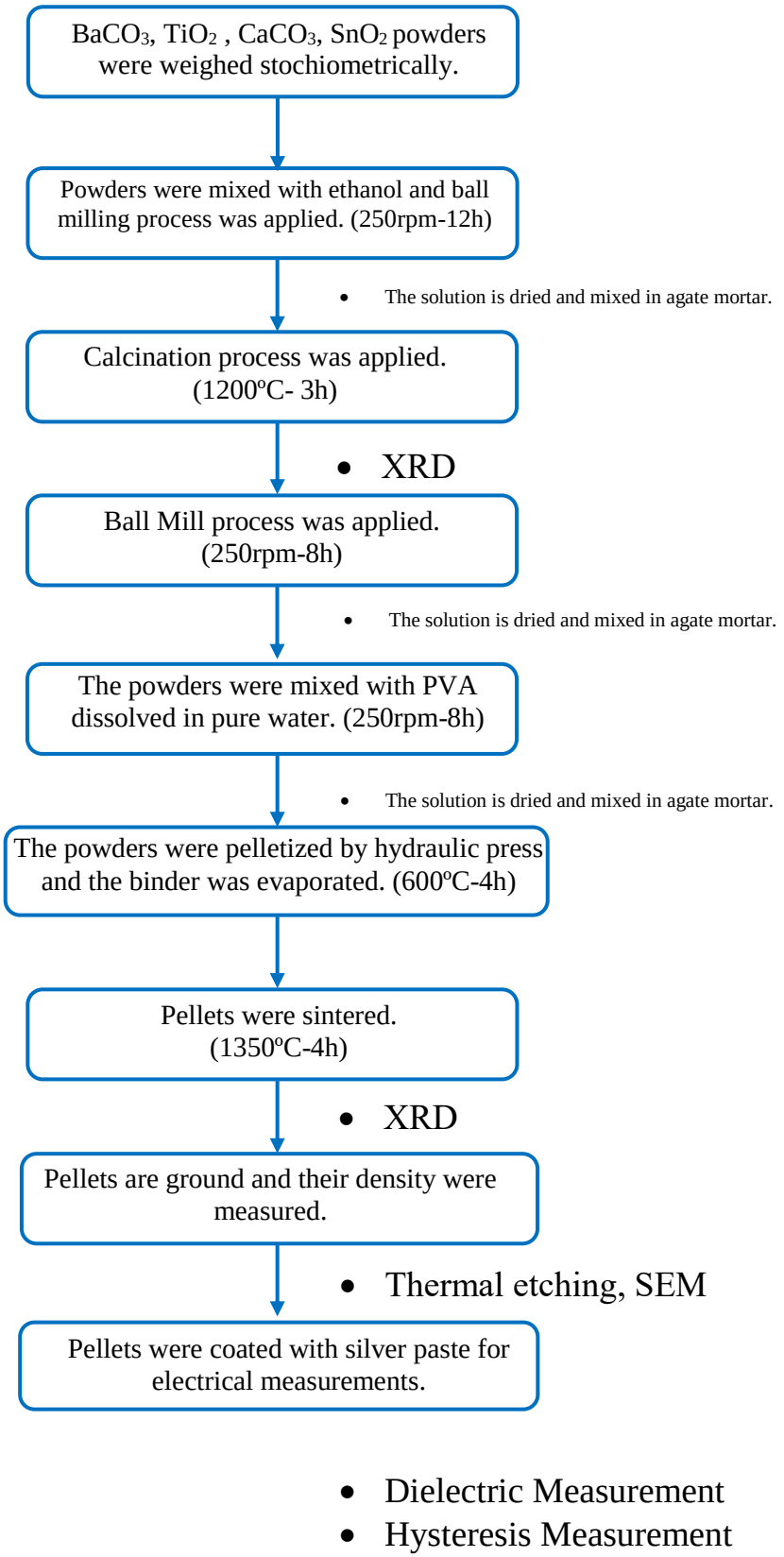

Figure 2. 1. Synthesis flow-chart of $Ba_{0.94}Ca_{0.06}Ti_{0.925}Sn_{0.075}O_3$

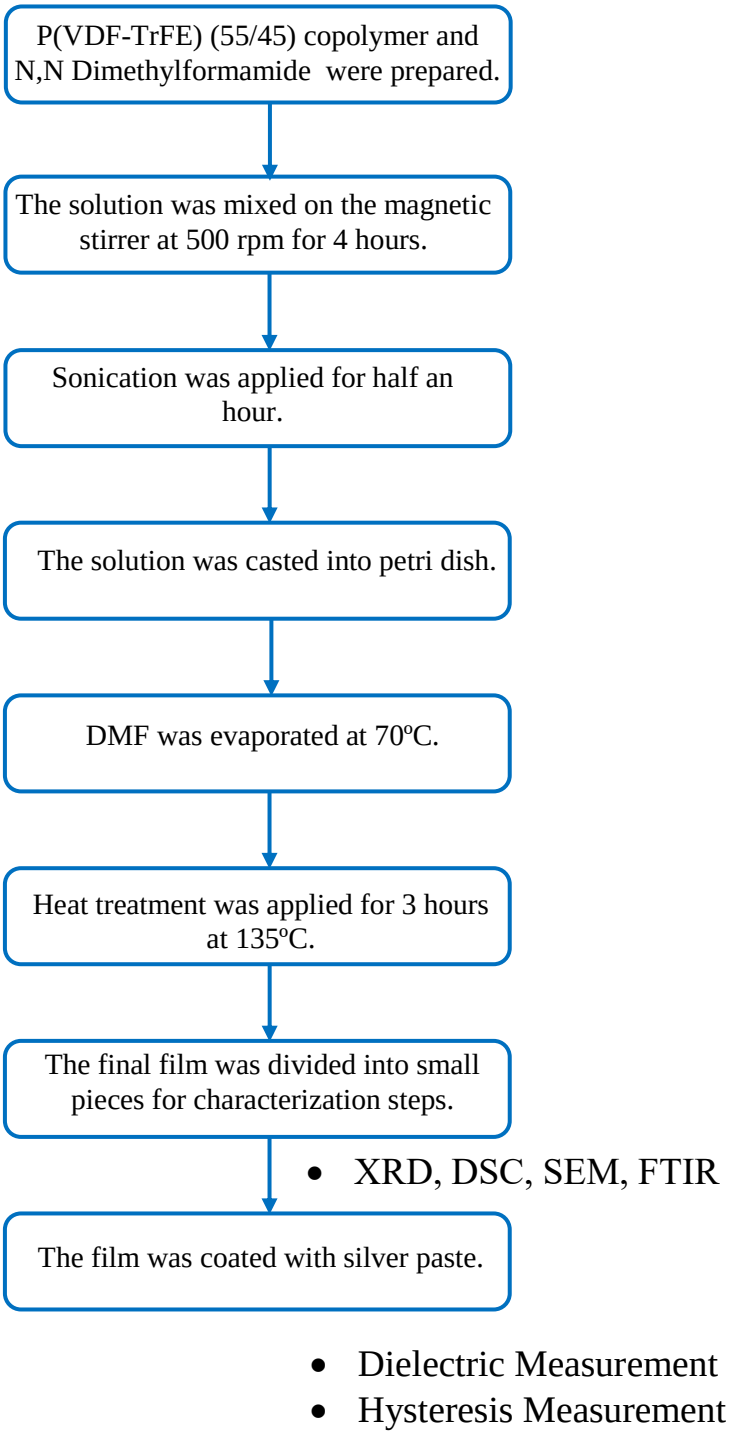

Figure 2. 2. Synthesis flow-chart of pristine P(VDF-TrFE) 55/45

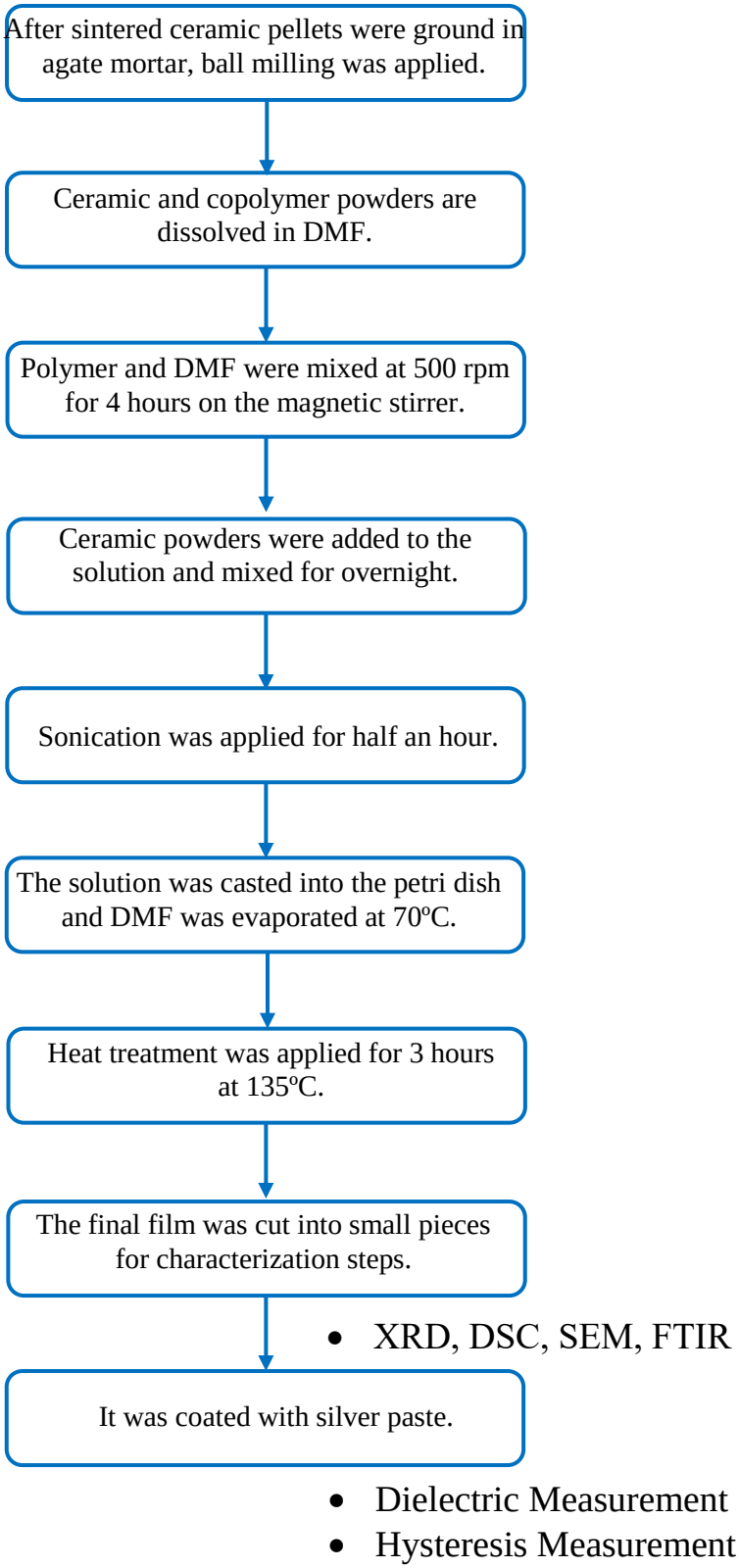

Figure 2. 3. Synthesis flow-chart of BCST- P(VDF-TrFE)55/45 composites

2.2.7. Dielectric Measurements

In order to characterize the electrical properties of the produced materials, dielectric properties measurements were done. Materials must be prepared for electrical characterization steps. For the electrical measurements, ceramics with 10 mm diameter and 1 mm thickness were polished and coated with silver paste (RS PRO RS:123-9911). The silver paste was dried at 135ºC for 7 minutes in the drying oven (Memmert UF55). In the sample preparation of polymer and composite films, silver paste was applied to rectangular cut samples (approximate thickness between 20-40µm) with the help of a mold with a diameter of 13 mm. The silver paste was dried at room temperature for 1 day.

Dielectric measurements were performed under AC Voltage at four different frequencies (100 Hz, 1 kHz, 10 kHz, 100 kHz) between 25°C - 150°C (TF 1000 temperature controller) by using on the LCR Meter (Keysight, E4980AL) and the data was collected by using a Lab-view program. The samples were placed in a sample holder filled with silicone oil (Aixacct piezo sample holder TFA 423-7), as the silicone oil prevents formation of sparks.

LCR meter measures the impedance of a circuit and converts it to Inductance, Resistance or Capacitance. The working principle of LCR meter is related to the concept of Impedance. Impedance (Z) consists of Reactance X_S (imaginary) and Resistance R_S (real) parts. Reactance is defined by $X_S = |Z| * \sin\theta$, resistance is defined by $R_S = |Z| * \cos\theta$.[71] For reactance to be capacitive, the θ angle must be less than zero, and to be inductive, the angle must be greater than zero. The LCR meter reads and displays the capacitance values of the materials in this context. Dielectric constant values were calculated using parallel plate capacitor equation. ε_r: relative permittivity, C: capacitance (F), d: thickness (mm), A: surface area (mm^2), ε_0: vacuum permittivity (8.854×10^{-12} F/m).

$$\varepsilon_r = \frac{C * d}{A * \varepsilon_0} \qquad (2.2.)$$

2.2.8. Ferroelectric Hysteresis Loop Measurements

In order to characterize the ferroelectric properties of the materials, the shape, behavior and polarization values (P_S, P_R) of the hysteresis loops were investigated. In

order to calculate the electrocaloric temperature change of samples indirectly by using Maxwell's equation, the change of the polarization with respect to temperature must be obtained. Hysteresis loops were measured using Aixacct TF Analyzer 1000 connected to TREK 610E High Voltage Amplifier.

The samples were placed into the sample holder filled with silicone oil and the measurements were performed between room temperature and the temperature at which linear hysteresis loops are obtained. For all samples(coated with silver paste), the amount of applied voltage (AC) was increased at regular intervals to reach the saturation point. Then the electric field was kept constant, and the temperature was increased in a stepwise manner. The temperature was increased until the hysteresis loops became completely linear. Measurements were performed at 10 Hz for ceramic pellets and at 100 Hz for thick films. In order to the calculate the electrocaloric temperature change, polarization as a function of temperature at constant electric field must be obtained based on the indirect method. The polarization values at each temperature were collected from second quadrant of hysteresis loop of materials at same electric field and P-T curve drawn. $((\partial P)/(\partial T))_E$ was obtained by using numerical equation (1.6) or by differentiating of the polynomial fitted P(T) curve. Then adiabatic temperature change of samples was calculated by inserting values of the$((\partial P)/(\partial T))_{\mathrm{E}}$, ρ, E, C_P and T of the samples in the 1.4 equation.

CHAPTER 3

RESULTS AND DISCUSSION

In this section, the structural and electrical characterization measurements of synthesized samples have been given and discussed.

3.1. Structural and Electrical Characterizations of BCST

Firstly, results of different characterization measurements of the filler part of the nano composites are given.

3.1.1. X-Ray Diffraction of BCST

Figure 3.1 demonstrates the XRD pattern of BCST ceramics. Impurity peak was not observed, and the XRD pattern of BCST shows the formation of pure perovskite structure.[64]

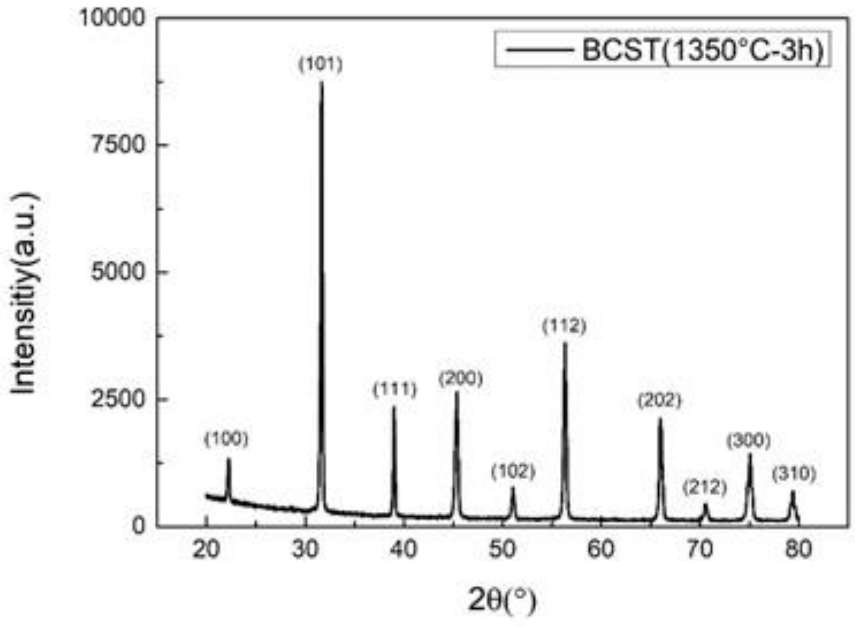

Figure 3.1. XRD pattern of $Ba_{0.94}Ca_{0.06}Ti_{0.925}Sn_{0.075}O_3$

3.1.2. Scanning Electron Microscopy Analysis of BCST

In order to visualize of microstructure of BCST ceramics, backscatter electron images were taken from the scanning electron microscopy. According to the backscatter images of BCST at the 2500x, which are given the figure 3.2, grains are formed properly, and grain sizes are almost similar for each of them. Average grain sizes was estimated as 30 µm.

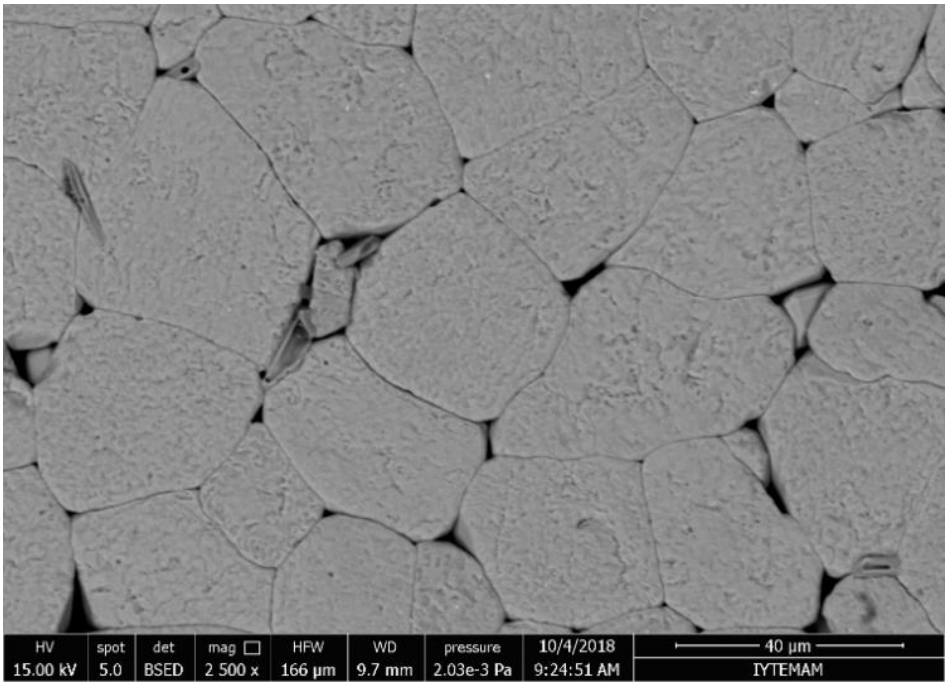

Figure 3.2. SEM images of $Ba_{0.94}Ca_{0.06}Ti_{0.925}Sn_{0.075}O_3$ ceramics at 2500x magnification

3.1.3. Dielectric Measurements of BCST

In order to understand ferroelectricity and phase transition behaviour of BCST, temperature dependent dielectric measurements were done with LCR meter and TF1000 Analyzer. Figure 3.3 demonstrates the dielectric constant and loss versus temperature graph between room temperature and 200 ºC at different frequencies. The ferroelectric paraelectric phase transition of BCST was observed at ~70ºC (Curie temperature). According to XRD measurements, there was a tetragonal orthorhombic phase transition for BCST, which has 0.0075 content of Sn, at room temperature.[72] A peak was observed in both dielectric constant and dielectric loss measurements at the room temperature, this

proved the tetragonal orthorhombic phase transition. Dielectric constant and loss values of BCST were very close to similar studies in the literature.[64]

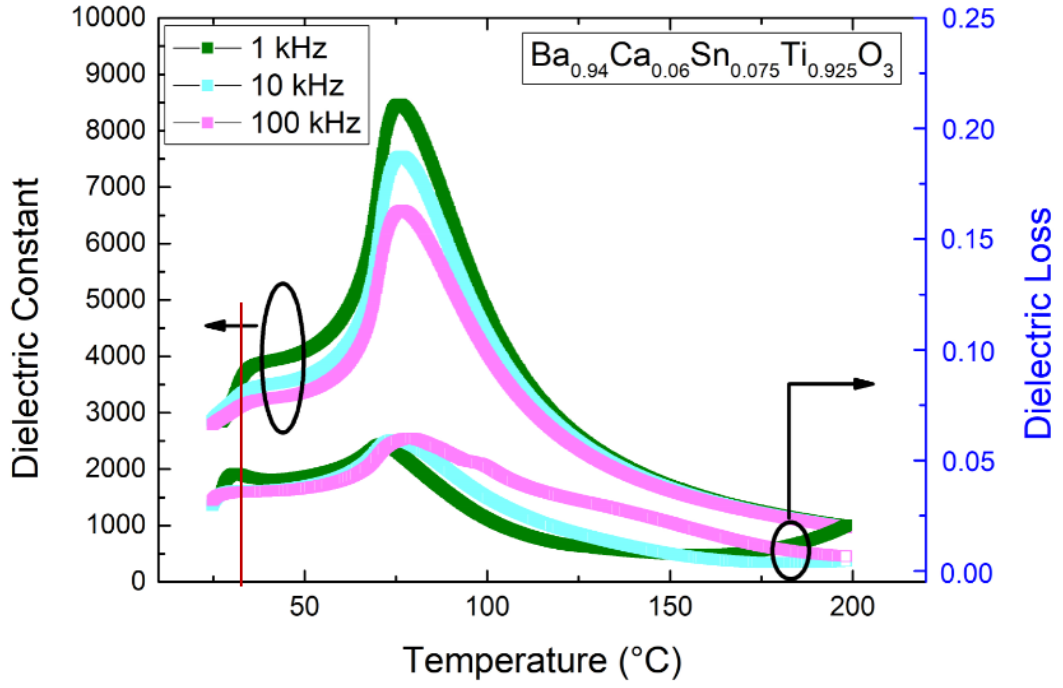

Figure 3.3. Dielectric Constant and Loss as a function of temperature of $Ba_{0.94}Ca_{0.06}Ti_{0.925}Sn_{0.075}O_3$ ceramics at 1 kHz, 10 kHz and 100 kHz.

3.1.4. Hysteresis Loop Measurements and ΔT Calculation of BCST

In order to calculate ECE with the indirect method, temperature dependent hysteresis loops of the samples were measured by using Aixacct TF Analyzer 1000. The hysteresis loop of BCST showed the ferroelectric behavior and maximum polarization of BCST was measured 18 μC/cm^2. Electrocaloric temperature change was calculated by using Maxwell's equations (1.4.). Density value of BCST ceramic was measured by based on Archimedes principle, and found the 5.66 g/cm^3. Specific heat capacity value was taken from other studies, a 500 Jkg/K.[73-75] Figure 3.4 indicates the hysteresis loop, polarization and ΔT versus temperature behavior of BCST at 5, 10, 15, 20 kV/cm electric field at 10 Hz frequency. Maximum adiabatic temperature change was obtained 0.42 K at 20 kV/cm at Curie temperature region due to ferroelectric paraelectric phase transition. ΔT peak at the room temperature is related with the orthorhombic to tetragonal phase transition.

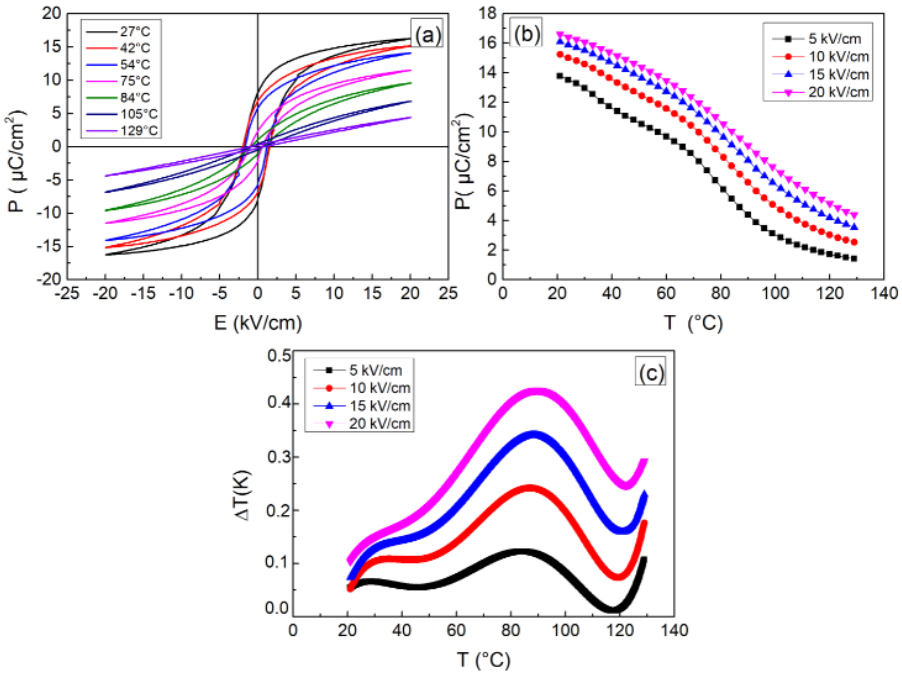

Figure 3.4. (a)P(E) loops at different temperature, (b) P(T) and (c)ΔT vs T graphs of $Ba_{0.94}Ca_{0.06}Ti_{0.925}Sn_{0.075}O_3$.

3.1.5. Particle Size Analysis of BCST

The main aim of ball milling, which was applied to sintered ceramic, is to reduce the particle size to the nanometer scale as much as possible. The milled particle size of final ceramic powder was obtained between 100 and 200 nm. Particle size distribution of reinforcement phase obtained from DLS experiment given the figure 3.5.

3.2. P(VDF-TrFE) and P(VDF-TrFE)-BCST Characterizations

In this section, the results of characterization experiments of thick films which are 5, 7.5, 10 volume percent of BCST added composites and pristine copolymer will be discussed.

5, 7.5, 10 volume percent of ceramic powder were chosen in the composite thick films. Figure 3.6 indicates that volume percent of both polymer and ceramic parts corresponding to the weight percent.

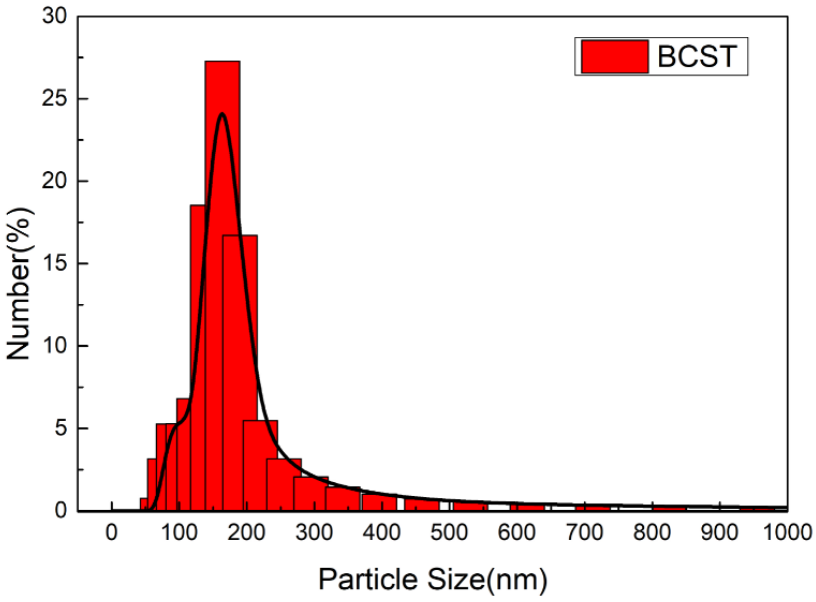

Figure 3. 5. The particle size distribution of $Ba_{0.94}Ca_{0.06}Ti_{0.925}Sn_{0.075}O_3$

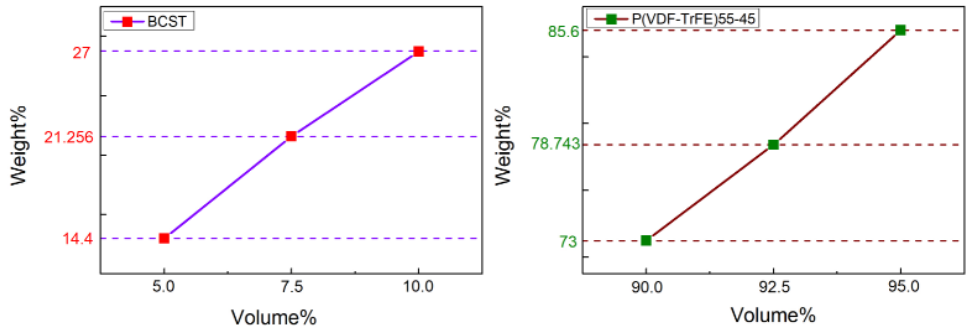

Figure 3.6. Volume corresponding to weight percent ratios of both $Ba_{0.94}Ca_{0.06}Ti_{0.925}Sn_{0.075}O_3$ and P(VDF-TrFE) 55-45 in the composites.

3.2.1. X-Ray Diffraction Measurements of Thick Films

The crystalline phases and chain conformation of pristine polymer and composites were obtained by using X-ray diffraction characterization method. Indirect method was used for ECE calculation in this study, so it is important that the material have the ferroelectric properties. Figure 3.7 demonstrates X-ray diffraction patterns of BCST, pristine copolymer, and composites (5, 7.5, 10vol% BCST) normalized moreover the characteristic 2θ region of copolymer are given to show how the polymer changes with

the ceramic powder addition. P(VDF-TrFE) copolymer have the some characteristic peak belongs to ferroelectric phase. These peaks are shown at 2θ: 19.2º and 18.7º belongs to (110) and (200) planes (non-polar α phase), and (110) planes indicate the β crystalline phase (polar phase), which has ferroelectric chain conformation (TTT zig-zag), of copolymer.[45] According to our results, there was a broad peak at the 19.2º degree, so this proved that the beta phase of copolymer was obtained. The semi crystalline behavior brings about wide pattern mechanism, because there is still amorphous phase in the polymer and composite materials. This shows that the final thick film products did not a hundred percent crystallinity.

The XRD pattern of composite materials gave not only polymer characteristic peak but also ceramic characteristic peaks. Increased ceramic powder addition brought about the shifted of polymer characteristic peak to lower angles, moreover the nonpolar phase of copolymer has also been formed. To understand the appearance of the nonpolar phase in composite and copolymer characteristic peak shifting, d spacing values of (110) planes for all thick films were calculated by using Bragg's law: $\lambda = 2d\sin\theta$. The d inter chain spacing values of pristine polymer, Comp5vol%, Comp7.5vol%, Comp10vol% at the (110) plane (polar phase of copolymer) were found as 4.5620, 4.6454, 4.6612, 4.6771 respectively. When the amount of BCST nanoparticles increases, the inter chain spacing increases, it can be explained with the decrease of the ferroelectric phase of copolymer.[76] XRD peak shifting is associated with increasing of the inter chain spacing, thus this shows that phases are close to paraelectric state and proved ferroelectric behavior of the materials.[77] In addition, increasing of inter chain distance of copolymer with ceramic filler addition can causes ferroelectric domain size of polar phase become smaller, but this does not indicate that the ferroelectric phase is not found.[78] Another approach about lattice spacing increasing and splitting of copolymer characteristic pattern was suggested by Liu et al. They investigated how the different VDF volume content of P(VDF-TrFE) copolymer could affect the properties of the copolymer. They claimed that VDF content, which was between 49 and 55, had morphotropic like behavior due to the peak splitting among these VDF contents. (200) planes belongs to 3-1 helical chain conformation and (110) planes belongs to TTT chain conformation. The presence of both type of chain conformation in the crystal structure was explained with morphotropic phase like behavior by Liu et al.[79]

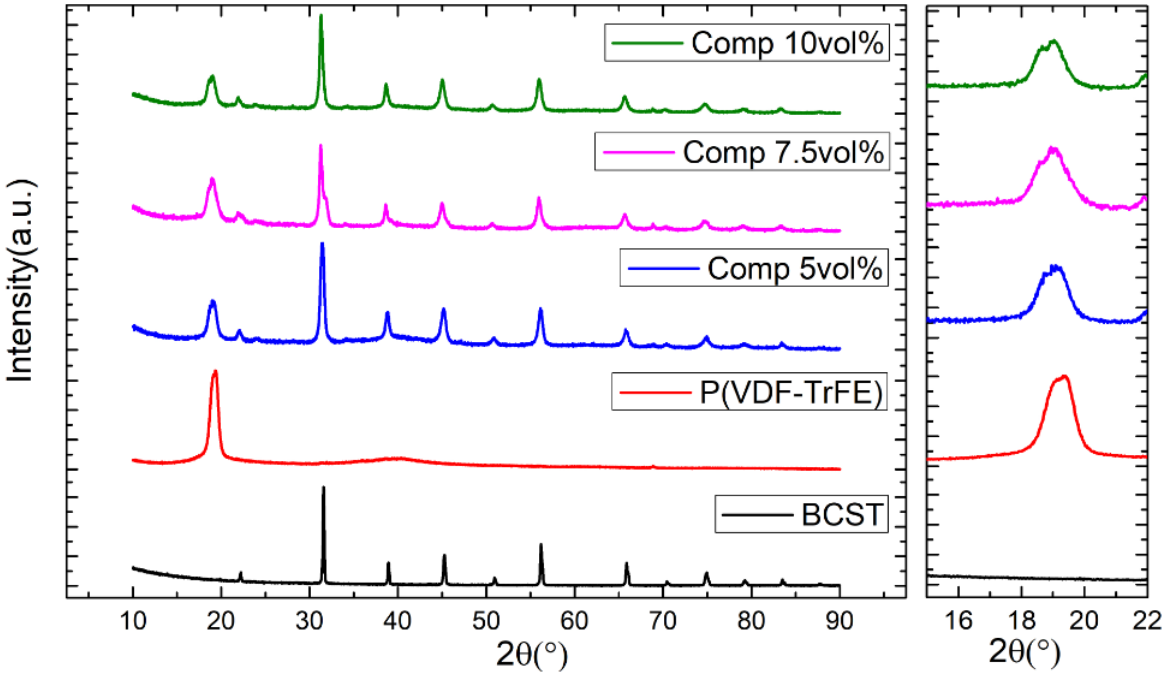

Figure 3.7. The XRD patterns of $Ba_{0.94}Ca_{0.06}Ti_{0.925}Sn_{0.075}O_3$, P(VDF-TrFE)55-45, Comp(5 vol% BCST), Comp(7.5 vol% BCST) and Comp(10 vol% BCST) and between 2θ: 15-22º.

3.2.2. Fourier Transform Infrared Spectroscopy of Thick Films

In order to understand bond vibration modes and functional groups of molecules in the polymer chain and ceramic crystal structure, ATR Fourier Transform Infrared Spectroscopy measurements were done. Figure 3.8 demonstrates transmittance signals of synthesized ceramic powder, pristine copolymer and composite thick films. The β phase signals of P(VDF-TrFE) copolymer are C-H_2 and C-F_2 stretching vibrations which given the signals at 1285 and 847cm^{-1} wavelength.[80] According to the FTIR transmittance analysis results, our pristine copolymer give characteristic signals of the beta phase. The characteristic FTIR signals of $BaTiO_3$ based ceramics are Ti-O vibration and CO_3 stretching at ~594 and 1447cm^{-1} wavelength.[81] The Ti-O vibration of Sn and Ca co doped BT give the signal at 500 cm^{-1} wavenumber lower the pure BT, Ca and Sn doping can leads to Ti-O vibration signals shifting.[82]

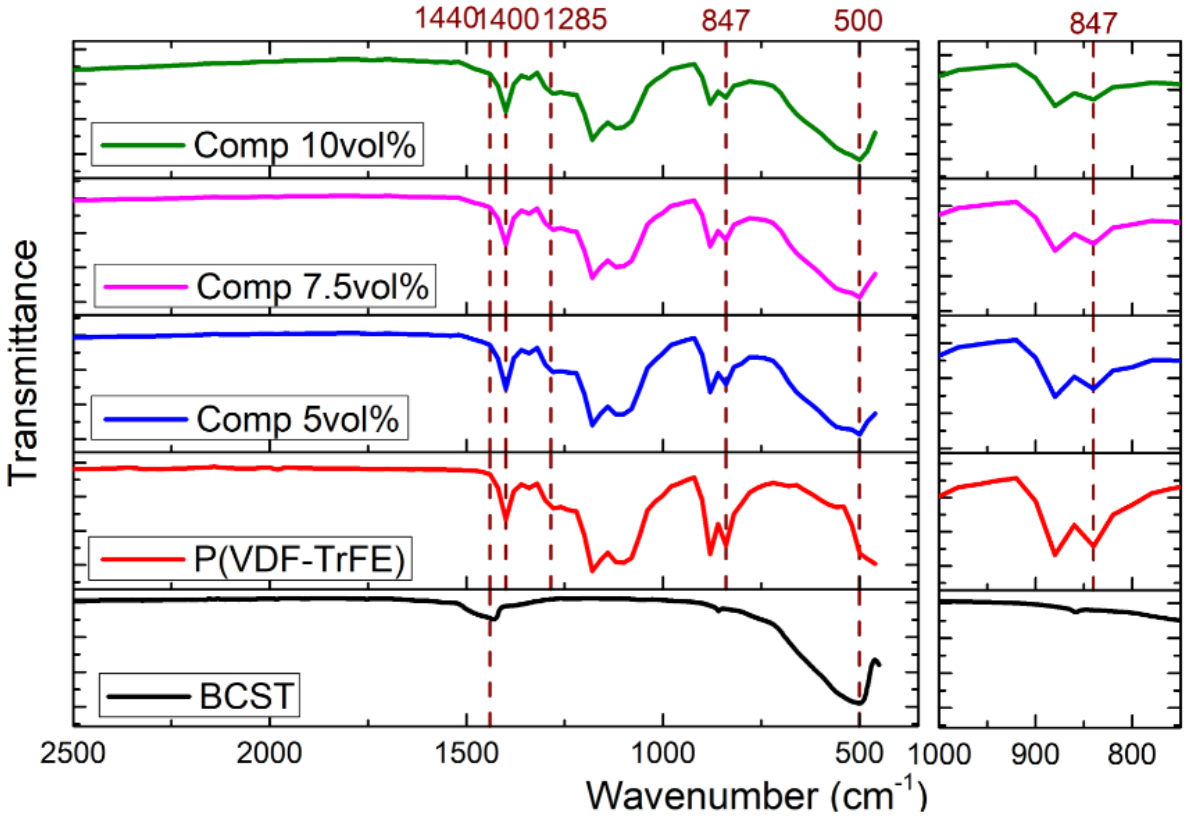

Figure 3.8. The transmittance signals of $Ba_{0.94}Ca_{0.06}Ti_{0.925}Sn_{0.075}O_3$, P(VDF-TrFE)55-45, Comp(5 vol% BCST), Comp(7.5 vol% BCST) and Comp(10 vol% BCST) between 2500 and 400 cm^{-1}.

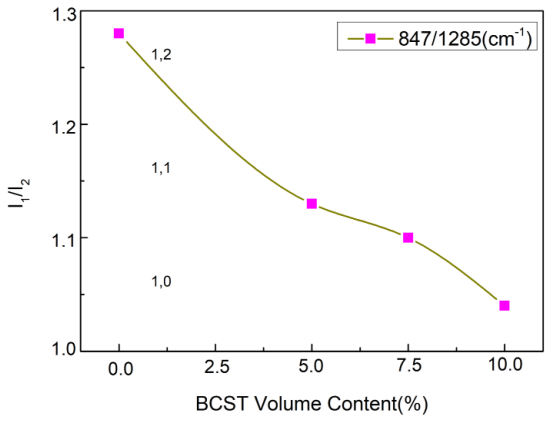

Figure 3. 9. C-F_2/ C-H_2 vibrations intensities ratios versus BCST filler content.

Doping of some elements to A site and/or B site of $BaTiO_3$ decreases the Curie temperature, and this reflects on Ti-O vibration wavenumber. The study of Utara et.al. on Ca and Zr co doped $BaTiO_3$ ceramic shows that Ti-O vibration signal of this material was

at the 560 cm^{-1} wavenumber, this indicates that doping mechanism decreases the vibration signal wavenumber.[82]

In addition, the 879 cm^{-1} belonged to the amorphous phase of copolymer.[83] The ceramic filler content increasing in the composites decreases the intensity of the amorphous copolymer a phases, but the intensities of the others vibration and stretching signals also reduces. In order to understand why intensity of signals decrease, the intensities of stretching C-F_2 (847cm^{-1}) and C-H_2 (1285cm^{-1}) vibrations were divided by each other. The comparison of ratios for pristine copolymer, and composites are shown the figure 3.9. When the ceramic filler content increases in the composites, CF_2/CH_2 intensity ratio decreases. Ceramic powders and polymer chain are found together in the composites, and they have to wet well each phase to another for obtaining a good composite. This wetting mechanism can creates Van der Walls connection between them and, therefore causes large interfacial interactions.[84]

3.2.3. Scanning Electron Microscopy of Thick Films

In order to understand the microstructure, morphology and cross section of all produced thick films, like sintered ceramic pellets, scanning electron microscopy was used. Cross section images were taken for the estimation of the thickness of thick films. To understand of the distribution of ceramic powders in the polymer matrix, back scatter electron images were taken at different magnification. Figure 3.10 shows that the Back Scatter images of pristine copolymer (a), 5vol% filler added composite (b), 7.5vol% filler added composite (c), and 10vol% filler added composite at 5.000x. Figure 3.11 also demonstrates the 10.000x for the same samples. According to SEM images, different volume content of BCST nanoparticles are distributed in polymer matrix homogenously, moreover the agglomeration is not seen in any samples. Homogenous distribution implies strong adhesion between ceramic and polymer parts, so this creates high level of interfacial connection between them.[85] When we compare to other similar studies, which studies polymer (matrix part) ceramic (reinforcement part) nanocomposite, the distribution of ceramic powders into polymer matrix is better in our case. [86-88]

Figure 3.12, 13, 14, 15 demonstrate the cross section images of thick film samples broken with liquid nitrogen. The thickness of the samples were estimated by SEM images.

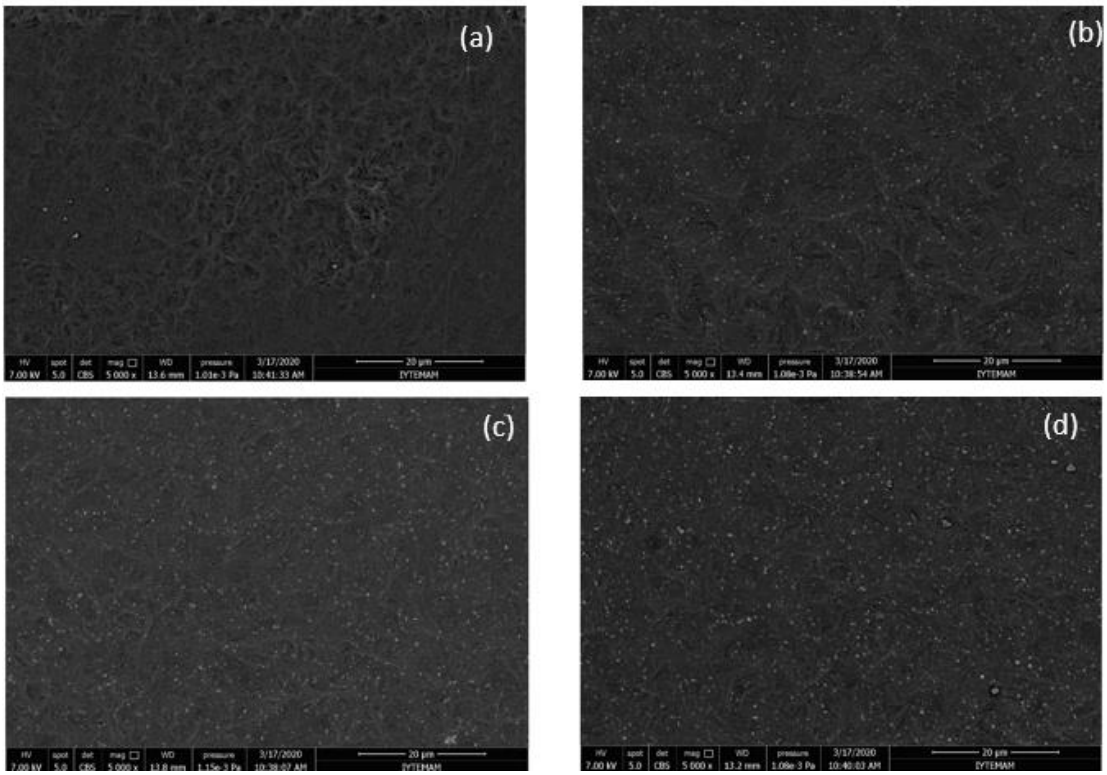

Figure 3. 10. The surface SEM images of (a) pristine P(VDF-TrFE), (b)Comp(5 vol% BCST) (c) Comp (7.5 vol% BCST), (d) Comp (10 vol% BCST) at 5.000x.

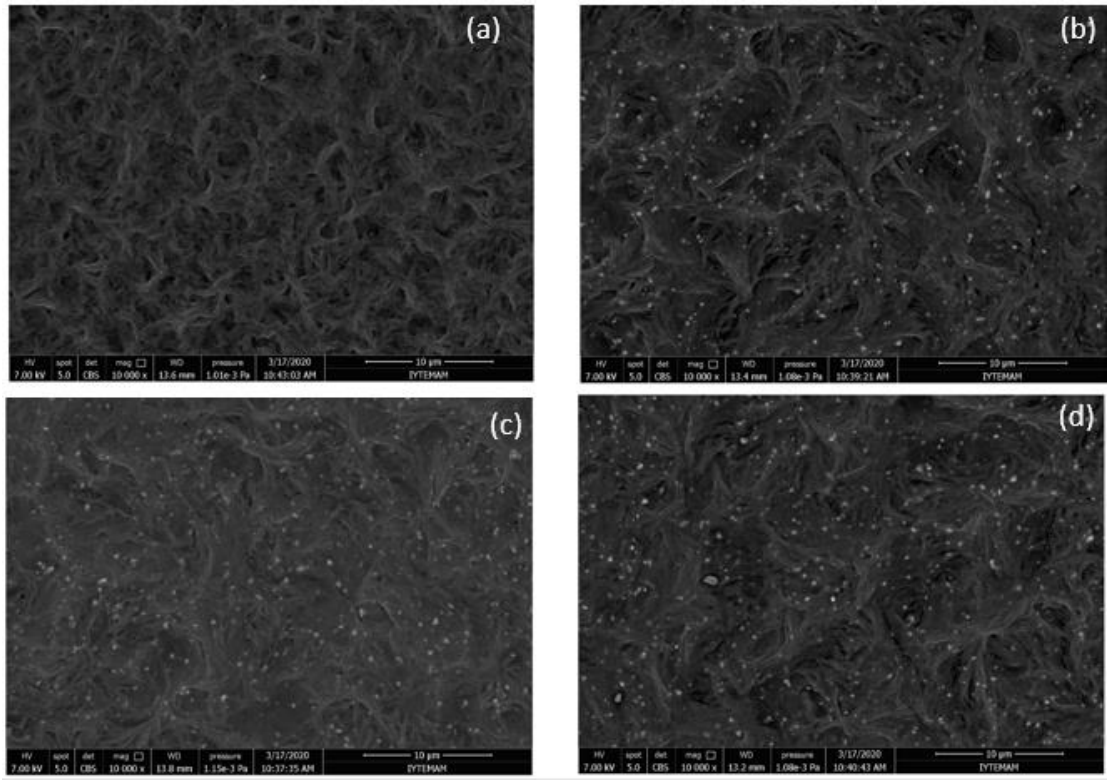

Figure 3.11. The SEM images of (a)pristine P(VDF-TrFE), (b) Comp(5 vol% BCST), (c) Comp (7.5 vol% BCST), (d) Comp (10 vol% BCST) at 10.000x.

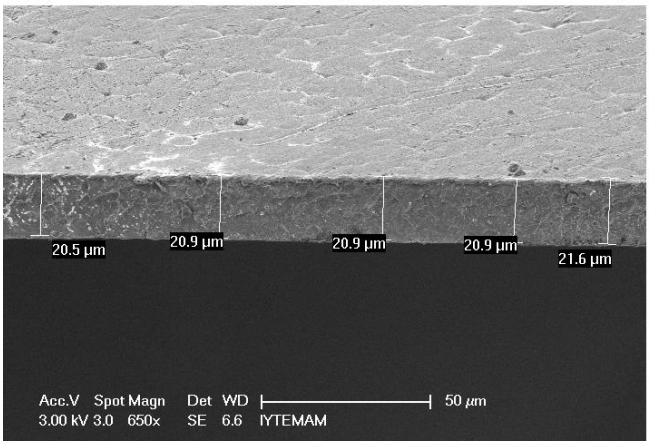

Figure 3.12. Cross section image of P(VDF-TrFE) 55-45 thick film (average thickness: 21µm).

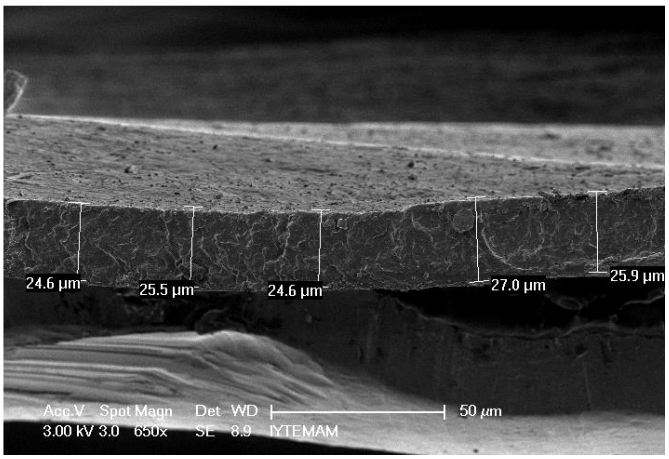

Figure 3. 13. Cross section image of Comp5 vol% BCST thick film (average thickness: 26µm).

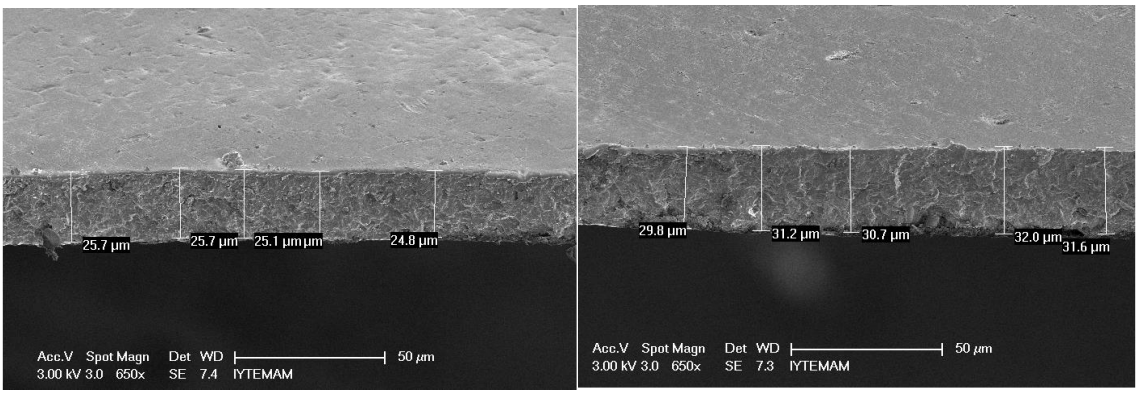

Figure 3. 14. Cross section image of Comp7.5 vol% BCST thick film (average thickness: 28µm).

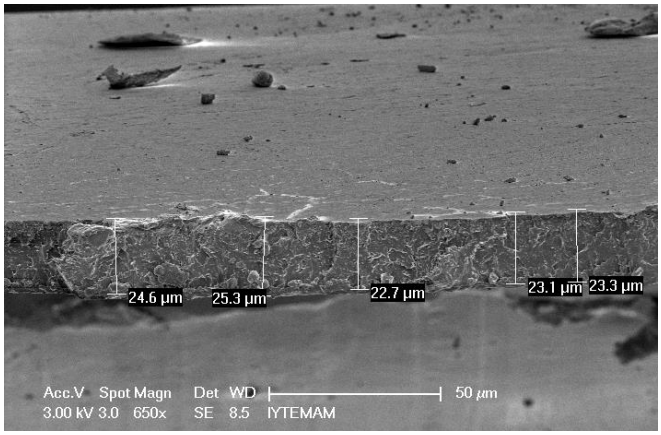

Figure 3. 15. Cross section image of Comp10 vol% BCST thick film (average thickness: 24 µm).

3.2.4. Differential Scanning Calorimetry of Thick Films

The amount of energy absorbed or released was measured with DSC equipment. Clear patterns were obtained for the composites, which contains polymer part, that's why energy changes of polymer was more than ceramics. Figure 3.16 demonstrates DSC heating curves of 0, 5, 7.5, 10 volume percent of BCST composites at the Curie temperature region. According to this graph, increasing of filler content brought about shifting to low temperature (similar to other studies[89, 90]), because reduction of polymer volume fraction decreases enthalpy of polymer.[91]

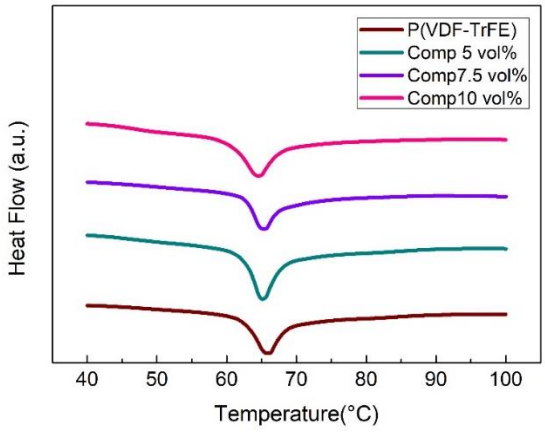

Figure 3.16. The DSC heating curves of P(VDF-TrFE)55-45, Comp(5 vol% BCST), Comp(7.5 vol% BCST) and Comp(10 vol% BCST).

3.2.5. Dielectric Measurements of Thick Films

The first step of electrical characterization is the dielectric properties measurement. In order to calculate the values of dielectric constant value calculation, parallel plate capacitor formula (2.2) was used. The dielectric constants of all produced samples autwere calculated based on this formula, by using a Lab-view program.

There are many approaches of 0-3 type of polymer ceramic composite dielectric constant calculation. Some of them are Jaysundere-Smith Equation (3.1.), Modified Lichtnecker Equation (3.2.), Series mixing formula (3.3.), Maxwell Wagner Equation (3.4.), and Effective Medium Theory (3.5.).[92]

$$\varepsilon_{eff} = \frac{\varepsilon_m(1-vf) + \varepsilon_i vf \left[\frac{3\varepsilon_m}{\varepsilon_i 2\varepsilon_m}\right]\left[\frac{1+3vf(\varepsilon_i-\varepsilon_m)}{\varepsilon_i+2\varepsilon_m}\right]}{1-vf+vf\left[\frac{3\varepsilon_m}{\varepsilon_i+2\varepsilon_m}\right]\left[\frac{1+3vf(\varepsilon_i-\varepsilon_m)}{\varepsilon_i+2\varepsilon_m}\right]} \quad (3.1.)$$

$$\log \varepsilon ff = \log \varepsilon_m + vf(1-n)\log\left(\frac{\varepsilon_i}{\varepsilon_m}\right) \quad (3.2.)$$

$$\frac{1}{\varepsilon_{eff}} = \frac{vf}{\varepsilon_i} + \frac{(1-vf)}{\varepsilon_m} \quad (3.3.)$$

$$\varepsilon_{eff} = \varepsilon_m \frac{2\varepsilon_m + \varepsilon_i + 2vf(\varepsilon_i-\varepsilon_m)}{2\varepsilon_m + \varepsilon_i - vf(\varepsilon_i-\varepsilon_m)} \quad (3.4.)$$

$$\varepsilon_{eff} = \varepsilon_m\left[1 + \frac{vf(\varepsilon_i-\varepsilon_m)}{\varepsilon_m + n(1-vf)(\varepsilon_i-\varepsilon_m)}\right] \quad (3.5.)$$

Temperature dependent dielectric measurement were done between room temperature and 150ºC for thick films. The melting temperature of copolymer materials is 158 ºC. Figure 3.17 shows that dielectric constant- dielectric loss versus temperature graphs for all solution casted thick films at 1, 10 and 100 kHz. There was a net ferroelectric paraelectric phase transition at Curie temperature for all thick film samples. The transition temperature T_C does not shift with increasing frequency for all samples showing the ferroelectric behavior, this proves the normal ferroelectric (and not relaxor ferroelectric) behavior of these samples. This is very important for calculation of the

electrocaloric temperature change by using indirect method. Dielectric constant versus temperature behavior of the composites are similar to pristine polymer, and dielectric behavior of composites is dominated by polymer matrix. Above the curie temperature the value of dielectric loss of all thick film samples increase at low frequency range, this could be related to enhanced the mobility of some impurity ions.[93]

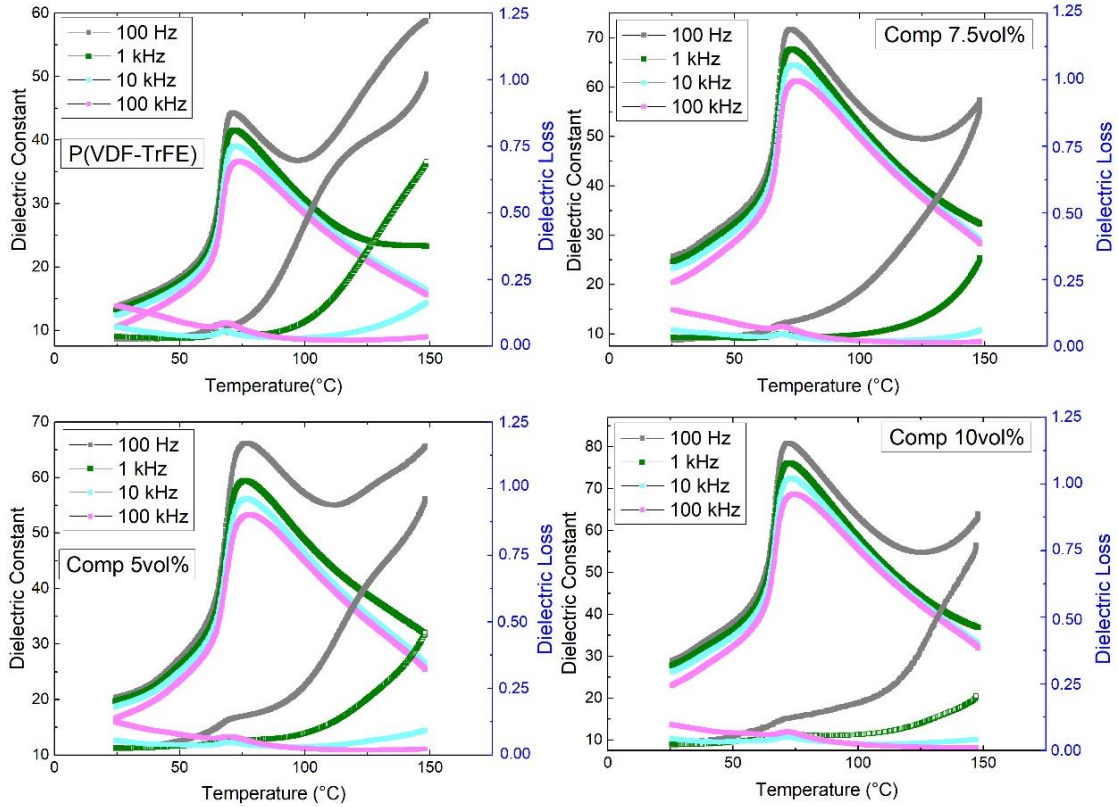

Figure 3.17. Dielectric permittivity and Tanδ versus temperature graph of P(VDF-TrFE)55-45, Comp(5 vol% BCST), Comp(7.5 vol% BCST) and Comp(10 vol% BCST) at 1,10 and 100 kHz.

Figure 3.18 shows the comparison of dielectric constant, tangent loss versus temperature behaviors of pristine copolymer, 5, 7.5, 10% volume content ceramic filler added thick films. The dielectric permittivity of pristine copolymer is generally between 10 and 15 values at the room temperature.[94, 95] Maximum dielectric constant values are obtained at the Curie temperature region, and this is three times of value, which is at the room temperature, in the literature.[21] Maximum dielectric constant value of our pristine copolymer was measured 40 at the 1 kHz, which was approximately three times of value at room temperature. Dielectric constant increased and dielectric loss reduced with BCST

ceramic filler addition, this is shown that the polymer ceramic composites.[88, 96-98] Maximum dielectric constant (ε_{max}) of 0, 5, 7.5, 10% volume content thick films were found 40, 60, 67, 76, which is the almost twice of pristine copolymer dielectric constant , moreover the Curie temperature of samples were found 71.7, 76.3, 73.4, 72,4ºC respectively at 1kHz frequency. The Curie temperature of the composites did not change systematically with filler addition, and this is not common in composite systems.[99] As previously mentioned that there are many theoretical calculation methods for 0-3 type of composite systems. When the dielectric constant was calculated by using theses equations, Maxwell Wagner and Jayesundere Smith gives the closest-results. Figure 3.19 shows the comparison between theoretical estimation and measured dielectric constant. Maxwell Wagner equations gives the correct dielectric constant for composites having low volume content ceramic filler[100], so dielectric constant of comp5vol% is very close to theoretical calculation with Maxwell Wagner equation. However, the differences between theoretical and measured dielectric constant increases with high content filler addition. Jayesundere-Smith equation is also reasonable for estimation of the dielectric constant of 0-3 type composites. According to this model, the spherical shape of particles added to polymer matrix, and it is necessary that there is good connection between the ceramic fillers which are well distributed in the polymer matrix).[101] In polymer ceramic composite systems, interfacial polarization and space charges increases dielectric constant at low frequencies, but this may change at high frequencies.[102] Enhancement of dielectric constant for our composites is observed at both low and high frequencies. Therefore, we cannot say the reason of improvement due to space charge or interfacial polarization.

3.2.6. Hysteresis Measurements of Thick Films

Figure 3.20 demonstrates that saturated hysteresis loops and current density versus electric field curves of the thick film samples.

The comparison of P-E loops and I-E curves of thick films under 900 kV/cm electric field at 10 Hz are given the figure 3.21. Hysteresis loop shape of pure P(VDF-TrFE) copolymer was rectangular-like shaped, because the tilting effect slowly increases depending on frequency.[103] The maximum polarization value of pristine copolymer was found 4.3 $\mu C/cm^2$ at 900 kV/cm, this is close to literature results.[41, 95] The maximum and

remnant polarization increased and coercive field decreased with BCST filler addition into the polymer matrix.[104-106] The production of composites, which are defect free and have strong dipole-dipole interaction, is important for increasing polarization and decreasing coercive field.[107]

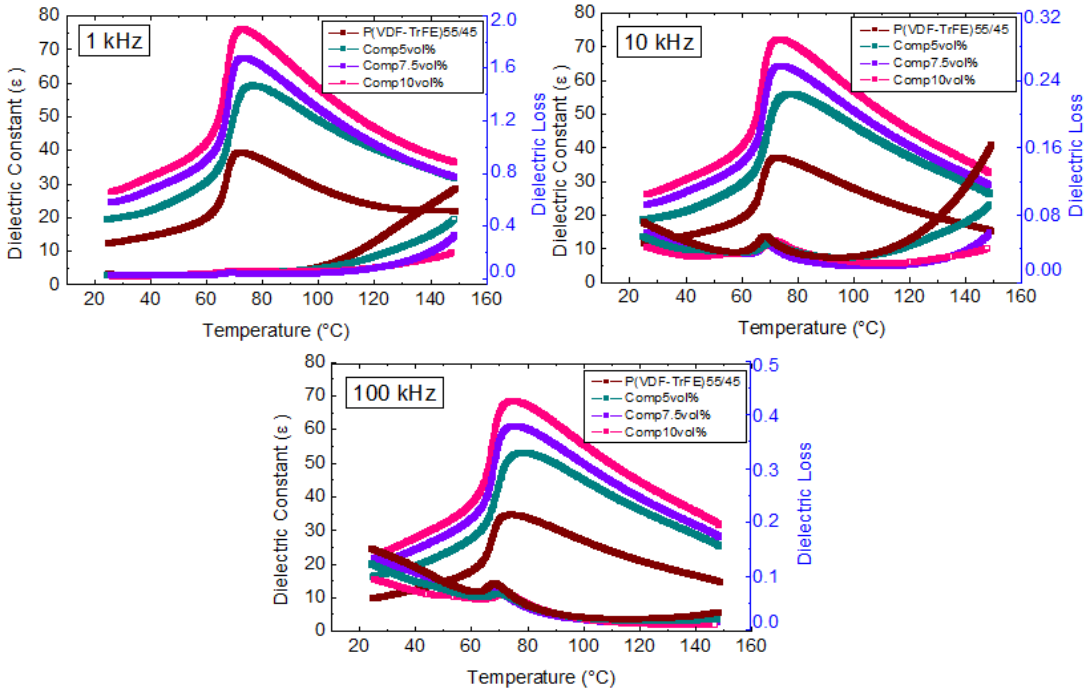

Figure 3.18. The comparison of dielectric constant, dielectric loss versus temperature graph of P(VDF-TrFE)55-45, Comp(5 vol% BCST), Comp(7.5 vol%BCST) and Comp(10 vol% BCST) at 1, 10 and 100 kHz.

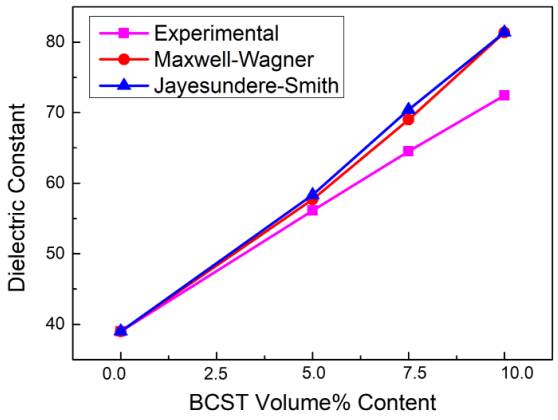

Figure 3.19. The comparison of experimental and calculated dielectric constant of composites with different volume content of BCST.

Table 3.1 demonstrates that remnant polarization (P_r), coercive field (E_c), maximum polarization (P_{max}), and Curie temperature (T_C) values of synthesized samples. The maximum polarization value of composite, which has 10 volume percent BCST, was measured 6.43μC/cm^2. It is approximately 1.5 times larger than that of the pristine copolymer. Remnant and maximum polarizations increases with addition of BCST particles, because of the amplifying effect of the ceramic of the polymer/ceramic interface. Ceramics, which has high dielectric constant need low electric field to polarized, in contrast to polymers, which have long chain configuration, need high amount of electric field. The other mechanism about enhancement of the polarization is the interfacial polarization. Interfacial polarization can form at the interface between the ceramic and the polymer, which can increase the polarization of composites.[17]

Current- Electric Field (I-E) behavior of ferroelectric materials shows time dependent domain switching, and it is crucial to obtain symmetrical current loop with well defined switching peaks in both negative and positive electric field.[108] Figure 3.21 (b) shows that the current increases with ceramic filler addition, similar to the polarization behavior.

3.2.7. Electrocaloric Temperature Change (ΔT) Calculation of Thick Films

The electrocaloric temperature change of the thick film samples were calculated with the indirect measurement methods, similar to BCST ceramics. In order to calculate adiabatic temperature change of materials, density and specific heat capacity of materials must be known. Used density and specific heat values of the ceramic part is given above the ceramic part results. 55-45 P(VDF-TrFE) copolymer density was accepted as 1.77g/cm3.[109] Furthermore, composite materials' densities were calculated using the composite mixing rule. The density of Comp5vol%, Comp7.5vol% and Comp10vol%, were used as 1.898, 1.997, 2.096 g/cm3 respectively.[110] The heat capacity value pristine copolymer was accepted as 2000 J/kgK in the Curie temperature region value from the other studies.[111] Composites' specific heat capacity values were calculated using the mixture rule, similar to the density calculation.[112] Calculated specific heat values of composites, which have 5, 7.5, 10 volume percent of BCST, were 1784, 1681, 1585 J/kgK respectively.

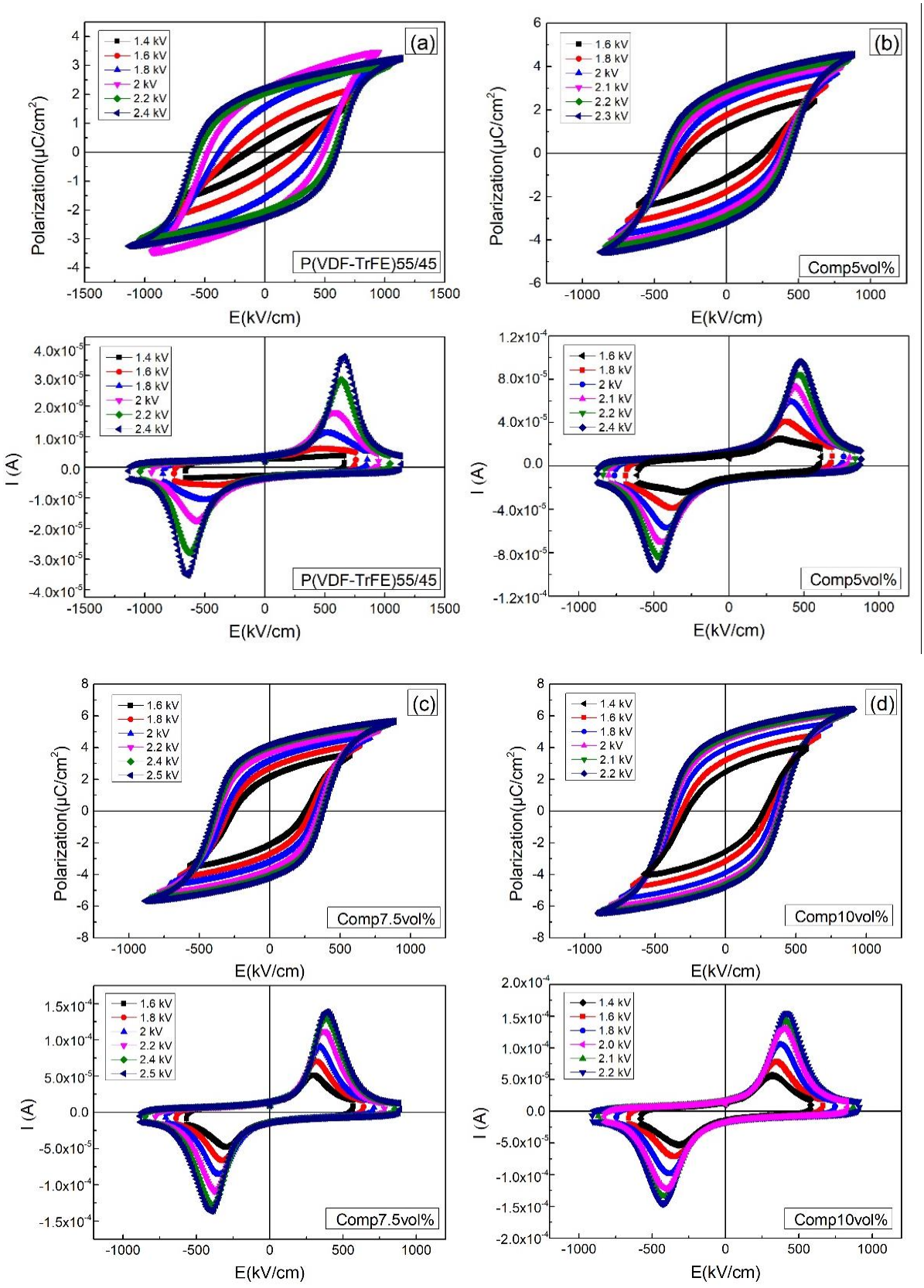

Figure 3. 20. P-E loops and I-E curves of (a) P(VDF-TrFE) 55-45, (b) Comp (5 vol% BCST), (c) Comp (7.5 vol% BCST), (d) Comp (10 vol% BCST)

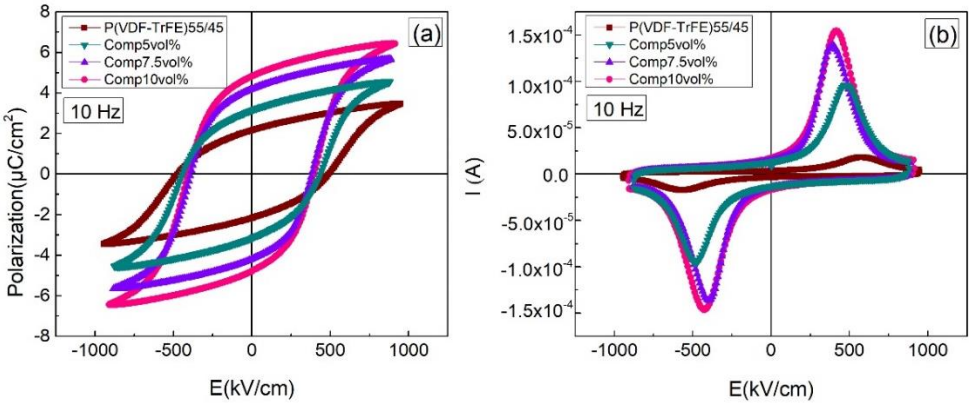

Figure 3. 21. Comparison of (a) P-E loops, (b) I-E curves of all thick film samples at 900 kV/cm electric field

Table 3.1 . P_r, P_m, E_C, T_C, ε_r and tanδ values comparison of P(VDF-TrFE) 55-45, Comp(5 vol% BCST), Comp(7.5 vol% BCST), Comp (10 vol% BCST)and $Ba_{0.94}Ca_{0.06}Ti_{0.925}Sn_{0.075}O_3$.

Materials	P_r (μC/cm2)	P_{max} (μC/cm2)	E_C (kV/cm)	T_C (°C)	ε_r (1kHz)	tanδ (1kHz)
P(VDF-TrFE) 55-45	2.15	3.5	466	71.7	40	0.69
Comp(5vol% BCST)	3.14	4.55	435	76.3	60	0.44
Comp(7.5vol% BCST)	4.18	5.66	389	73.4	67	0.37
Comp(10vol% BCST)	4.81	6.43	396	72.4	76	0.22
$Ba_{0.94}Ca_{0.06}Ti_{0.925}Sn_{0.075}O_3$	8.28	16.41	1.55	75.9	8470	0.020

Figure 3.22, 3.23, 3.24 and 3.25 show the temperature dependent hysteresis loops, P(T) and ΔT vs. T graphs of pristine P(VDF-TrFE) 55-45, Comp5vol%, Comp7.5vol% and Comp10vol% respectively. P(T) (fitted and non-fitted) and ΔT-T (sixth grade polynomial fitted) comparison of all thick film samples under 100, 500, and 900 kV/cm electric fields are shown in figure 3.23. Addition of the ceramic filler increases polarization and also the slope of the P(T) curve, therefore adiabatic temperature changes increases accordingly. In other words, electrocaloric effect improved with ceramic filler addition to the polymer matrix, similar to the other studies.[43, 45, 60, 61, 63] Maximum adiabatic temperature change of the composites was found to be 4.414 K (P(VDF-TrFE)), 5.903K (Comp5vol%), 6.38K(Comp7.5vol%) and 6.964K(Comp10vol%) at 900 kV/cm. There was a systematic improvement of ECE.

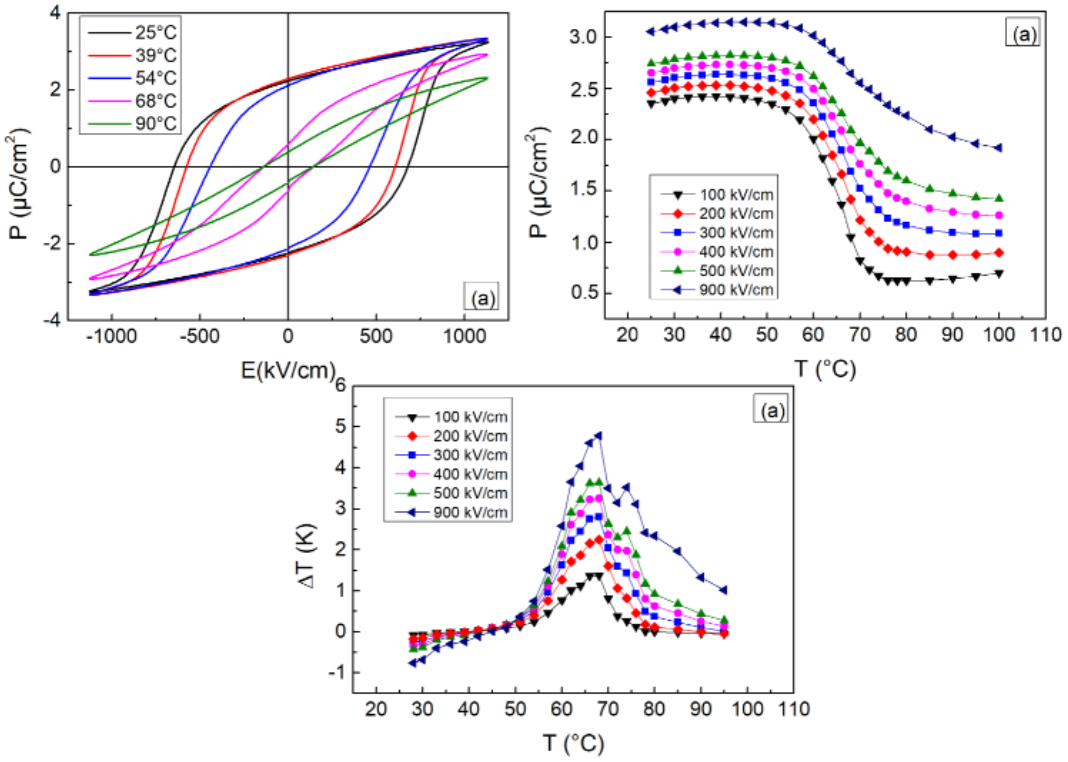

Figure 3.22. Temperature dependent P-E loops, P(T) and ΔT graphs of Pristine polymer

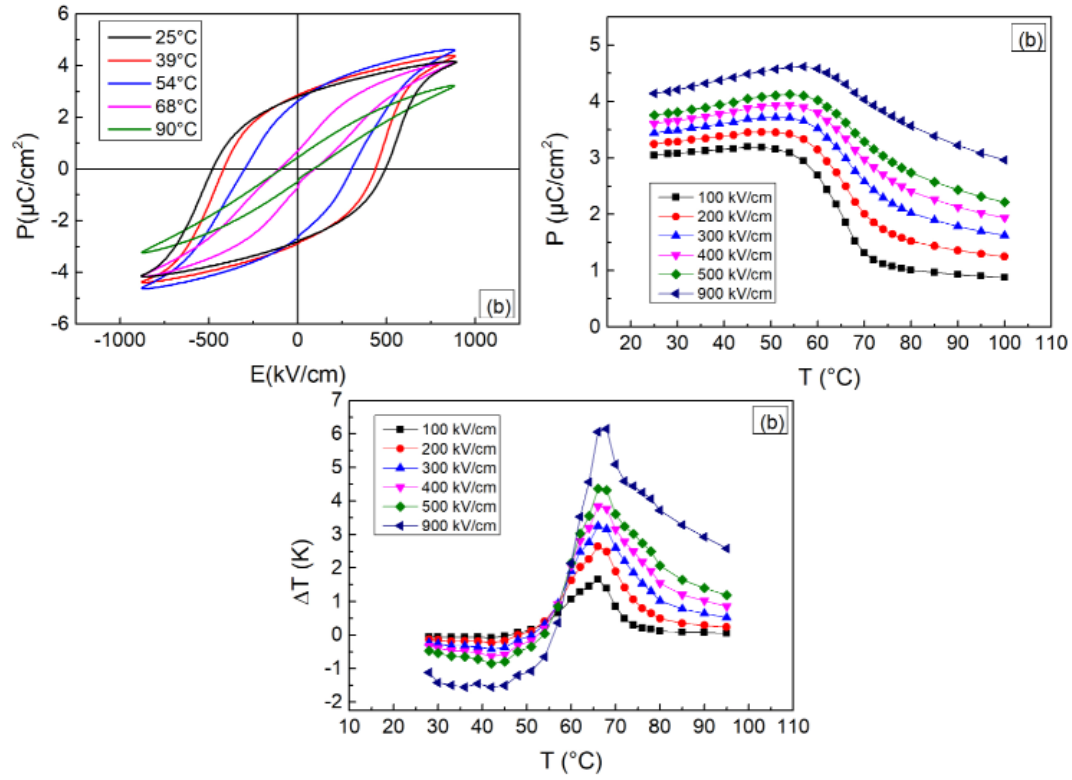

Figure 3.23. Temperature dependent P-E loops, P(T) and ΔT vs T graphs of Comp(5 vol%BCST)

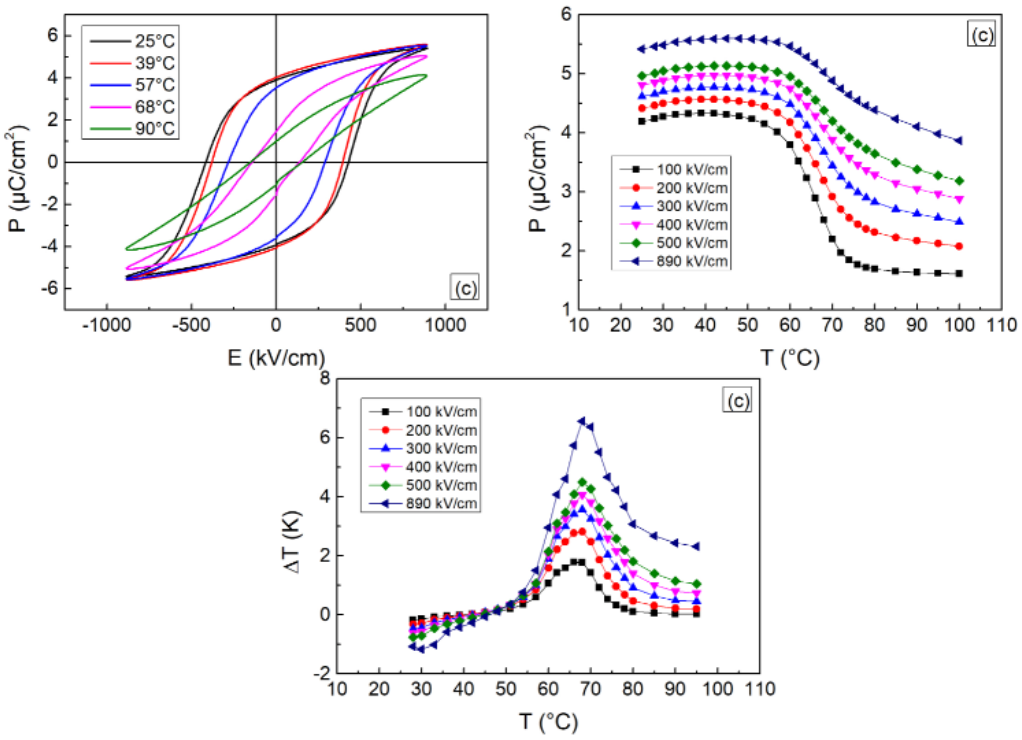

Figure 3.24. Temperature dependent P-E loops, P(T) and ΔT vs T graphs of Comp(7.5 vol%BCST)

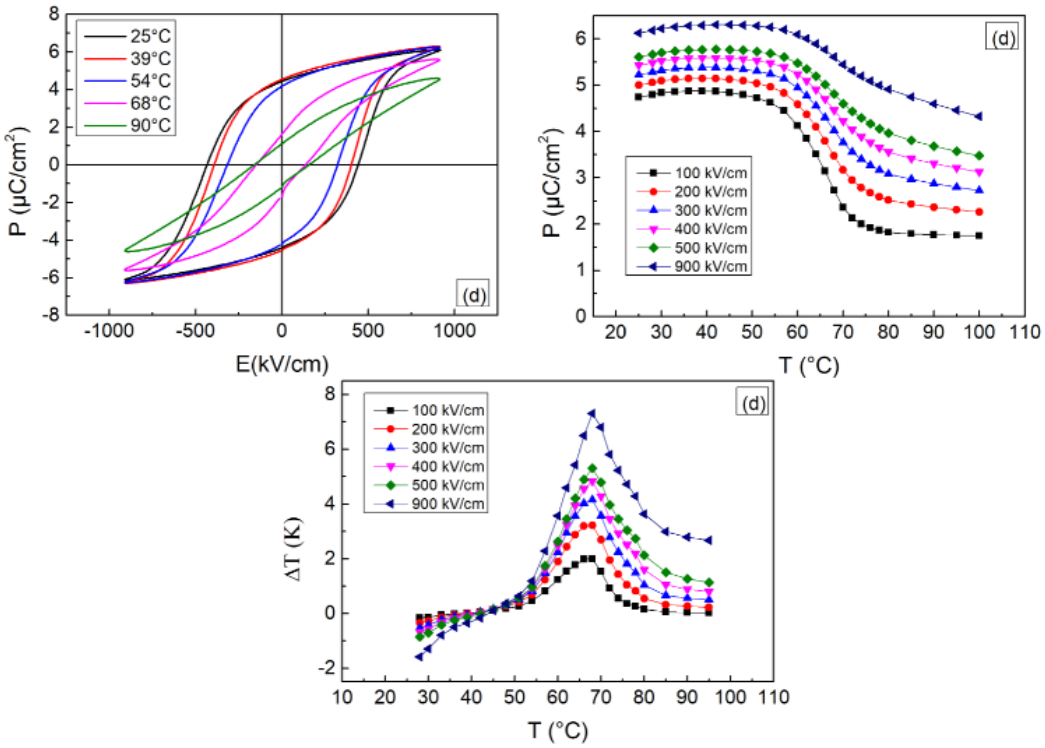

Figure 3.25. Temperature dependent P-E loops, P(T) and ΔT vs T graphs of Comp(10 vol%BCST)

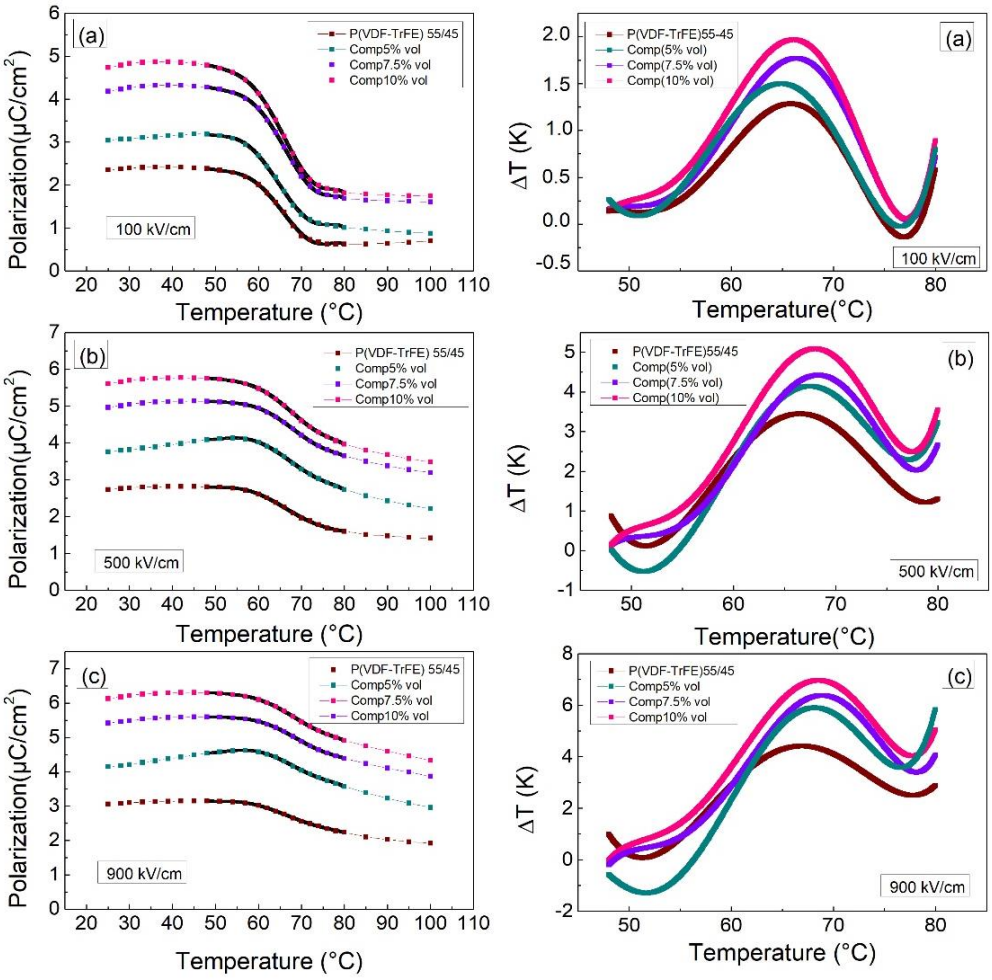

Figure 3.26. The comparison of P(T) and ΔT vs T curves obtain by fitting the P(T) curves with a 6th degree polynomial at (a)100 kV/cm, (b) 500 kV/cm, (c) 900 kV/cm

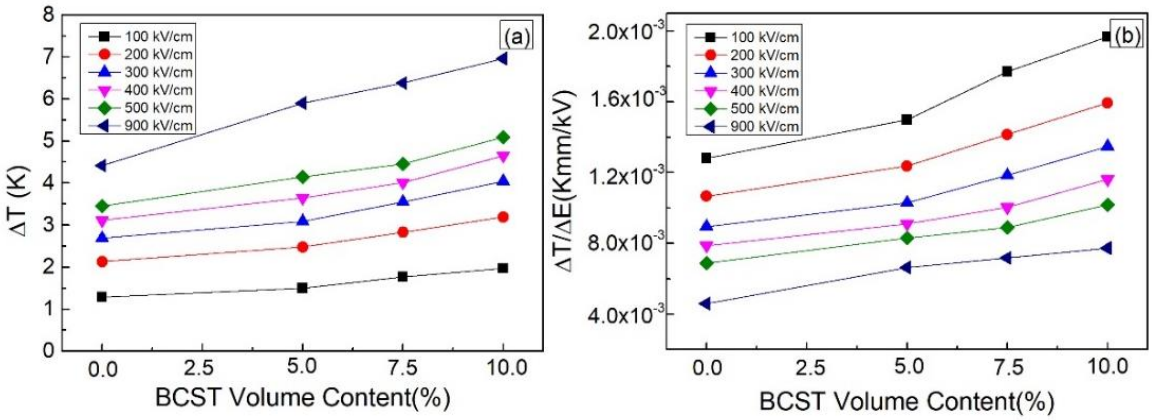

Figure 3.27. (a) ΔT and (b) ΔT /ΔE as a function of BCST volume content values of solution casted thick films under different electric field.

Isothermal entropy changes can be useful the in the design of electrocaloric cooling systems. Generally, isothermal entropy changes of ceramic materials are lower, because of the small ionic displacements in ferroelectric ceramics, so this causes the low entropy changes.[41] Isothermal entropy changes were calculated with Maxwell's equations based on indirect method. Figure 3.28 demonstrates that the entropy changes versus temperature behaviors of every thick film samples at 100, 500 and 900 kV/cm electric field. ΔS increases with ceramic filler addition, and the maximum ΔS was calculated as 68.19 J/kgK at 900 kV/cm for Comp10vol%.

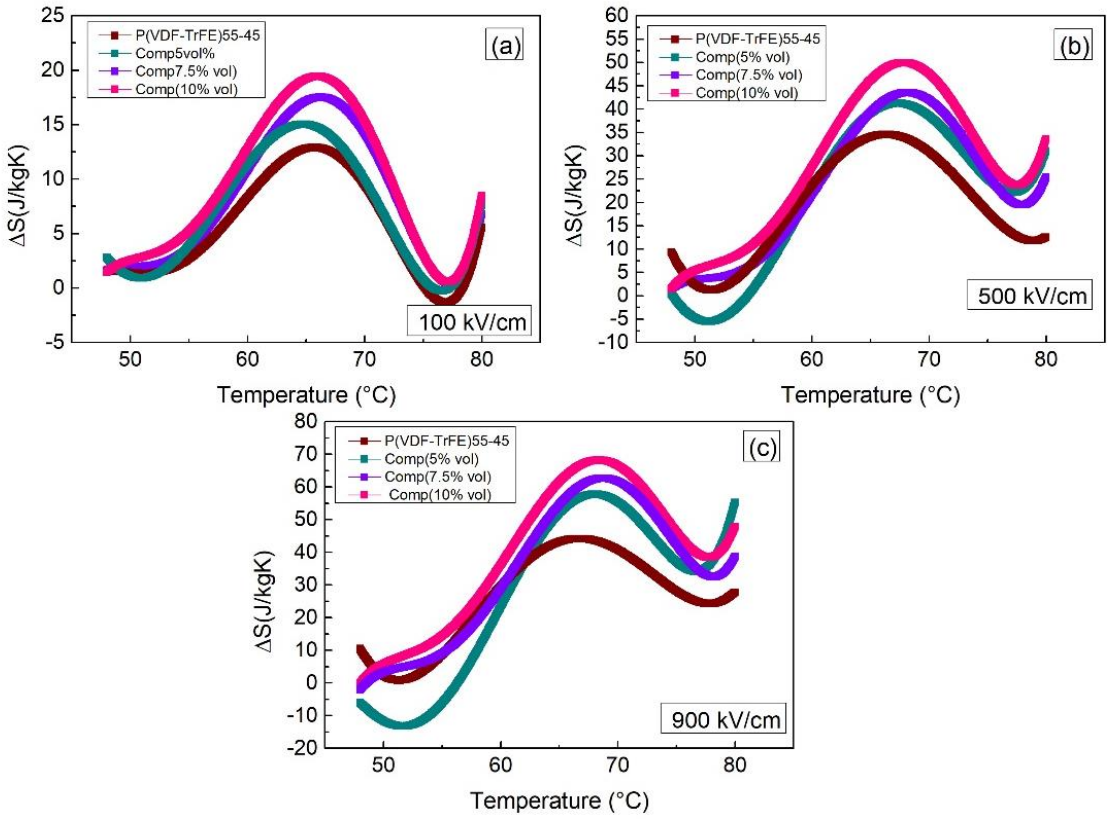

Figure 3.28. The comparison of ΔS vs T curves obtain by fitting the P(T) curves with a 6th degree polynomial at (a) 100kV/cm, (b) 500kV/cm, (c) 900kV/cm

Figure 3.29 indicates that isothermal entropy change and ΔS/ΔE values at different electric fields for each thick film samples. Addition of ceramic filler increased both isothermal entropy changes and ΔS/ΔE. Isothermal entropy change values of BCST ceramic phase were 0.961J/kgK (5 kV/cm), 1.88319 J/kgK (10 kV/cm), 2.64718 J/kgK (15 kV/cm), 3.29561 J/kgK (20 kV/cm).

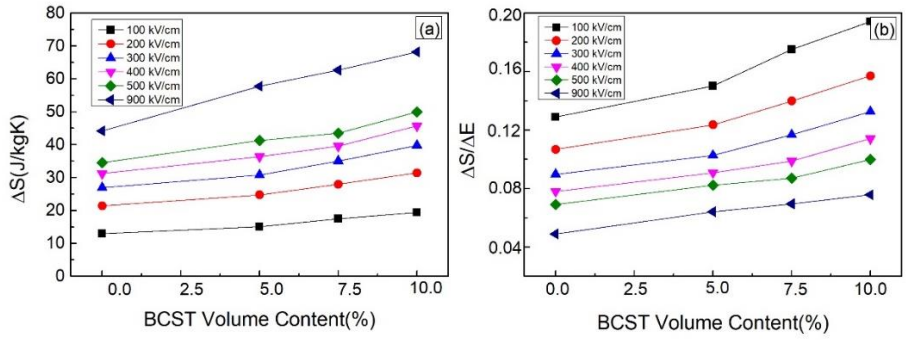

Figure 3.29. (a) ΔS and (b) ΔS / ΔE as a function of BCST volume content values of solution casted thick films under different electric field.

Table 3.2 includes a summary of electrocaloric properties of polymer thick films, polymer-polymer composites and polymer ceramic composites. Relaxor(terpolymer) - relaxor based composite systems were more commonly studied, because they show higher adiabatic temperature changes (in a broad temperature range) close to room temperature, and their ECE was measured by using direct method as they are relaxor ferroelectrics. Relaxors have nanodomains, which are not stable thermal and thermodynamically, therefore indirect method is not proper for the calculation of electrocaloric temperature change of relaxors. Direct measurements have some drawbacks for the accurate adiabatic temperature change calculation. One of them is that it is very difficult to provide adiabatic conditions. If the adiabatic conditions cannot be established, the value of electrocaloric temperature change cannot be obtained accurately by using direct method. Indirect method is suitable for non-relaxor based composite systems, which are normal ferroelectrics. We focused on the ferroelectric-ferroelectric based composite systems since their adiabatic temperature changes can be measured accurately by using indirect method. Moreover, in order to calculate ΔT using indirect method correctly, ferroelectric hysteresis loop must be saturated demonstrating a normal ferroelectric behavior is obtained. Other studies on ferroelectric polymer based composite systems use non-saturated hysteresis loop for the calculations e.g; their adiabatic temperature change results are not accurate.[45] We obtained the saturated hysteresis loops for the ferroelectric composites. The composite, which contains 10 volume percent of BCST, gave highest adiabatic temperature and isothermal entropy change. In addition, electrocaloric strength values are better than other similar studies on ferroelectric composites.

Table 3. 2. Electrocaloric properties comparison with the literature.

Material	ΔE (kV/cm)	ΔT (K)	ΔT/E (Kcm/kV)	ΔS (J/kgK)	ΔS/E	Method/ Material Type	Ref.
P(VDF-TrFE-CFE) (59.4/33.4/7.2 mol%) 0.9Pb($Mg_{1/3}Nb_{2/3}$)O_3-0.1PbTiO_3(37.5wt%)	750	9.4	0.0125	85	0.113	Direct-Relaxor	[43]
P(VDF-TrFE-CFE) (62.3/29.9/7.8mol%)-$Ba_{0.67}Sr_{0.33}TiO_3$(10vol%)	750		0.012	80	0.106	Direct-Relaxor	[57]
P(VDF-TrFE) (52/48)-$Ba_{0.75}Sr_{0.25}TiO_3$ (10vol%, 26wt%)	600	2.5	0.004	-	-	Indirect-Ferroelectric	[45]
P(VDF-TrFE-CFE) (62.5/29/8.5mol%)-P(VDF-TrFE) (55/45)(5vol%)	750	3.5	0.0046	-	-	Direct-Relaxor	[56]
P(VDF-TrFE-CFE) (62.5/29/8.5mol%)-P(VDF-TrFE) (55/45)(10vol%)	750	5	0.0066	-	-	Direct-Relaxor	[56]
P(VDF-TrFE-CFE) (61.3/30.5/8.2mol%) – $BaZr_{0.2}Ti_{0.8}O_3$(5vol%)	900	7.4	0.00986	30	0.033	Direct-Relaxor	[61]
P(VDF-TrFE-CFE) (62.3/29.9/7.8mol%) – BNNs-BST-1-2-3	2000	35	0.0175	310	0.155	Direct-Relaxor	[60]
P(VDF-TrFE-CFE) (63.2/29.7/7.1mol%) – $BaTi_{0.89}Sn_{0.11}O_3$(7.5vol%)	1000	9	0.009	79	0.079	Indirect-Relaxor	[63]
P(VDF-TrFE-CFE) (62.3/29.9/7.5mol%) – $Ba_{0.67}Sr_{0.33}TiO_3$(NPs,NCs, NCR)	1000	14	0.014	120	0.12	Direct-Relaxor	[44]
P(VDF-TrFE) (55/45)	1200	8	0.0066	26	0.021	Indirect-Ferroelectric	[21]
P(VDF-TrFE-CFE) (62.5/29/8.5mol%) – ZrO_2 (3vol%)	1400	9.2	0.00657	46	0.032	Direct-Relaxor	[113]
P(VDF-TrFE) (55/45)	2090	12	0.00574	55	0.026	Indirect-Ferroelectric	[41]
P(VDF-TrFE) (55/45)	900	4.4	0.0046	44.172	0.049	Indirect-Ferroelectric	This work
P(VDF-TrFE)-BCST(5%vol)	900	5.9	0.00663	57.737	0.064	Indirect-Ferroelectric	This work
P(VDF-TrFE)-BCST(7,5%vol)	900	6.3	0,00717	62.657	0.069	Indirect-Ferroelectric	This work
P(VDF-TrFE)-BCST(10%vol)	900	6.9	0.00773	68.188	0.075	Indirect-Ferroelectric	This work

3.3.Discussions of Results

Upon the addition of ceramic filler in to the polymer matrix, the electrocaloric temperature change (ΔT) and isothermal entropy change (ΔS) increases. There are different mechanisms in the literature about the enhancement of ΔT.

According to the similar studies, the interfacial coupling factor, which occurs between ceramic and polymer parts, leads to increase of the ECE. Interfacial coupling can be simply explained as the following: Ceramics which are polarized at lower electric field will amplify the applied electric field and increase the effective electric field acting on the polymer matrix at the interface between ceramic and the polymer, increasing the electrical polarization. In order to understand the interface effect, some research groups reported different experiments. Qiang et al. used the piezoelectric force microscopy to understand the effect of interfacial coupling factor on relaxor terpolymer and BZT (barium zirconium titanate) composites.[62] Concentration, size, shape and aspect ratio of ceramic particle are very important in the composite systems. There is a limit of concentration of ceramics for obtaining favorable ferroelectric properties. Above the percolation concentration, the ceramic fillers aggregate, and this caused the polarization and $\partial P/\partial T$ to decrease.[43] In order to understand the effect of the shape, size and aspect ratio of the fillers in the composite system, Zhang et al. used phase field model to assess the electric field distribution between fillers, which have different morphologies. They obtained the maximum electrocaloric temperature change with the nanowire filler having high aspect ratio. In our study, BCST ceramic fillers were distributed in polymer matrix very well, according to the SEM images. This may cause the high interfacial coupling effect between matrix and ceramic filler region, and this increases the thermal motion of dipole moment in the interfacial region, so $(\partial P)/(\partial T)$ and ΔT values of our composites increased. If the filler concentration of composite reach the percolation, the dielectric constant, polarization, and ΔT should have decreased due to the electric field intensity making it difficult to move to dipole moments ordering. This indicates that we have achieved the optimal amount of filler below the percolation concentration. The new experiments can be tried with above ten volume percent of ceramic filler addition, in order to find the percolation concentration of composite systems as the future work.

CHAPTER 4

CONCLUSION

In this thesis, ferroelectric polymer ceramic composites (P(VDF-TrFE)55-45-BCST) with different amount of BCST (0, 5, 7.5, 10 vol%) were synthesized using solution casting method in order to investigate their electrocaloric properties for electrocaloric cooling applications.

The structure of composites was checked using XRD and FTIR measurements. Homogenous distribution of the ceramic nanoparticles in the polymer matrix was confirmed using SEM images. Dielectric measurements showed that dielectric constant increases and dielectric loss decreases as BCST content increases in the composites. The hysteresis loops of ferroelectric ceramic polymer composites were saturated very well, in contrast to many other ferroelectric composite studies in the literature. Ferroelectric polarization also increased as BCST content was increased. Electrocaloric temperature change (ΔT) and isothermal entropy change (ΔS) of the samples were calculated using the indirect method. The maximum ΔT, $\Delta T/\Delta E$ (electrocaloric strength) and ΔS values were obtained for the composite, which has 10% volume BCST filler as 6.964K, 0.007Kcm/kV and 68.188J/kgK under applied 900 kV/cm by using the indirect method. These values are quite promising and must result from the large interfacial coupling effect due to the homogenous distribution of ceramic particles in polymer matrix.

REFERENCES

1. Shi, Junye, et al., 2019 *Electrocaloric cooling materials and devices for zero-global-warming-potential, high-efficiency refrigeration.* Joule, p.1801949.

2. Pandey, R.Kumar, 2019 *Fundamentals of Electroceramics: Materials, Devices, and Applications*.: John Wiley & Sons, ISBN: 1119057345.

3. Busch, Georg., 1987 *Early history of ferroelectricity.* Ferroelectrics,. **74**(1): p. 267-284.

4. Sessler, GM, 1981 *Piezoelectricity in polyvinylidenefluoride.* The Journal of the Acoustical Society of America. **70**(6): p. 1596-1608.

5. Kim, Tae Yun, Sung Kyun. Kim, and Sang.Woo. Kim, 2018 *Application of ferroelectric materials for improving output power of energy harvesters.* Nano convergence. **5**(1): p.30.

6. Liang, Longyue, et al., 2016 *One-dimensional ferroelectric nanostructures: synthesis, properties, and applications.* Advanced Science. **3**(7): p. 1500358.

7. Damjanovic, Dragan, 1998 *Ferroelectric, dielectric and piezoelectric properties of ferroelectric thin films and ceramics.* Reports on Progress in Physics. **61**(9): p. 1267.

8. Kasap, Safa and Peter Capper, 2017 *Springer handbook of electronic and photonic materials*.: Springer. ISBN:331948933X.

9. Bokov, Alexei and Zuo.-Guang. Ye, 2012 *Dielectric relaxation in relaxor ferroelectrics.* Journal of Advanced dielectrics,. **2**(02): p. 1241010.

10. Shvartsman, Vlademir V and Doru C. Lupascu, 2012 *Lead-free relaxor ferroelectrics.* Journal of the American Ceramic Society. **95**(1): p. 1-26.

11. Samara, Georg A., 2003 *The relaxational properties of compositionally disordered ABO3 perovskites.* Journal of Physics: Condensed Matter. **15**(9): p. R367.

12. Bain, Ashim Kumar and Prem Chand, 2017 *Ferroelectrics: Principles and applications*.: John Wiley & Sons.ISBN:3527805400

13. Fu, Desheng and Mitsuru Itoh, 2015 *Role of Ca off-centering in tuning ferroelectric phase transitions in Ba (Zr, Ti) O3 system.* Ferroelectric Materials—Synthesis and Characterization.

14. Kabra, Hemangi, HA Deore, and Pranati Patil, 2019 *Review on Advanced Piezoelectric Materials (BaTiO3, PZT)*.

15. Thakur, Vijay Kumar and Raju Kumar Gupta, 2016 *Recent progress on ferroelectric polymer-based nanocomposites for high energy density capacitors: synthesis, dielectric properties, and future aspects*. Chemical reviews. **116**(7): p. 4260-4317.

16. Ruan, Liuxia, et al., 2018 *Properties and Applications of the β Phase Poly (vinylidene fluoride).* Polymers. **10**(3): p. 228.

17. Xia, Weimin and Zhicheng Zhang, 2018 *PVDF-based dielectric polymers and their applications in electronic materials.* IET nanodielectrics. **1**(1): p. 17-31.

18. Martins, P., AC Lopes, and S. Lanceros-Mendez, 2014 *Electroactive phases of poly (vinylidene fluoride): Determination, processing and applications.* Progress in polymer science. **39**(4): p. 683-706.

19. Wan, Chaoying and Christoper Rys Bowen, 2017 *Multiscale-structuring of polyvinylidene fluoride for energy harvesting: the impact of molecular-, micro- and macro-structure.* Journal of Materials Chemistry A. **5**(7): p. 3091-3128.

20. Barbosa, Joao C., et al., 2018 *Recent advances in poly (vinylidene fluoride) and its copolymers for lithium-ion battery separators.* Membranes. **8**(3): p. 45.

21. Lu, Sheng Guo, et al., 2011 *Electrocaloric effect in ferroelectric P (VDF-TrFE) copolymers.* Integrated Ferroelectrics. **125**(1): p. 176-185.

22. Chu, Baojin, et al., 2006 *A dielectric polymer with high electric energy density and fast discharge speed.* Science. **313**(5785): p. 334-336.

23. Liu, Quiang, 2016 *Development of electrostrictive P (VDF-TrFE-CTFE) terpolymer for inkjet printed electromechanical devices*.

24. Guggilla, Padmaja and Ashok K. Batra, 2011 *Novel Electroceramic: Polymer Composites-Preparation, Properties and Applications*.: INTECH Open Access Publisher, ISBN:9533073527.

25. Kim, Philseok, et al., 2009 *High energy density nanocomposites based on surface-modified BaTiO3 and a ferroelectric polymer.* ACS nano,. **3**(9): p. 2581-2592.

26. Zhou, Tao, et al., 2011 *Improving dielectric properties of BaTiO3/ferroelectric polymer composites by employing surface hydroxylated BaTiO3 nanoparticles.* ACS applied materials & interfaces. **3**(7): p. 2184-2188.

27. Ioannou, G., A. Patsidis, and G. Psarras, 2011 *Dielectric and functional properties of polymer matrix/ZnO/BaTiO3 hybrid composites.* Composites Part A: Applied Science and Manufacturing. **42**(1): p. 104-110.

28. Newnham, RE, DP Skinner, and LE Cross, 1978 *Connectivity and piezoelectric-pyroelectric composites.* Materials Research Bulletin. **13**(5): p. 525-536.

29. Dias, CJ and DK Das-Gupta, 1996 *Inorganic ceramic/polymer ferroelectric composite electrets.* IEEE Transactions on dielectrics and electrical insulation. **3**(5): p. 706-734.

30. Adnan Islam, Rashed and Shashank Priya, 2012 *Progress in dual (piezoelectric-magnetostrictive) phase magnetoelectric sintered composites.* Advances in Condensed Matter Physics, ISSN:1687-8108.

31. Akdogan, E.Koray, Mehdi Allahverdi, and Ahmad Safari, 2005 *Piezoelectric composites for sensor and actuator applications.* IEEE transactions on ultrasonics, ferroelectrics, and frequency control. **52**(5): p. 746-775.

32. Guo, Mengfam, et al., 2019 *High-energy-Density ferroelectric polymer nanocomposites for capacitive energy storage: enhanced breakdown strength and improved discharge efficiency.* Materials Today, ISSN:1369-7021.

33. Mishra, Suvrajyoti, et al., 2019 *Advances in piezoelectric polymer composites for energy harvesting applications: A systematic review.* Macromolecular Materials and Engineering. **304**(1): p. 1800463.

34. Kutnjak, Zdravko, Brigita Rožič, and Rasa Pirc, 1999 *Electrocaloric effect: theory, measurements, and applications.* Wiley encyclopedia of electrical and electronics engineering,: p. 1-19.

35. Correia, Tatiana and Qi Zhang, 2014 *Electrocaloric materials.* New Generation of Coolers,. **34**.

36. Rožič, Brigita and Zdravko Kutnjak. 2009. *Giant electrocaloric effect in ferroelectric relaxor materials*. in *Proceedings of the 2009 SEM Annual Conference&Exposition on Experimental and Applied Mechanics* Vol:174, p.1-6.

37. Liu, Yang, James F. Scott, and Brahim Dkhil, 2016 *Direct and indirect measurements on electrocaloric effect: Recent developments and perspectives.* Applied Physics Reviews. **3**(3): p. 031102.

38. Mischenko, AS, et al., 2006 *Giant electrocaloric effect in thin-film PbZr0. 95Ti0. 05O3.* Science. **311**(5765): p. 1270-1271.

39. Luo, Zhengdong, et al., 2014 *Enhanced electrocaloric effect in lead-free BaTi1− xSnxO3 ceramics near room temperature.* Applied Physics Letters. **105**(10): p. 102904.

40. Li, Qiang, et al., 2016 *Large electrocaloric effect in (Bi0. 5Na0. 5) 0.94 Ba0. 06TiO3 lead-free ferroelectric ceramics by La2O3 addition.* Materials Research Bulletin. **74**: p. 57-61.

41. Neese, Bret, et al., 2008 *Large electrocaloric effect in ferroelectric polymers near room temperature.* Science,. **321**(5890): p. 821-823.

42. Liu, PF, et al., 2010 *Huge electrocaloric effect in Langmuir–Blodgett ferroelectric polymer thin films.* New Journal of Physics. **12**(2): p. 023035.

43. Li, Qi, et al., 2015 *Relaxor ferroelectric-based electrocaloric polymer nanocomposites with a broad operating temperature range and high cooling energy.* Advanced Materials. **27**(13): p. 2236-2241.

44. Zhang, Guangzu, et al., 2015*Colossal room-temperature electrocaloric effect in ferroelectric polymer nanocomposites using nanostructured barium strontium titanates.* ACS nano. **9**(7): p. 7164-7174.

45. Jiang, ZY, XC Zheng, and GP Zheng, 2015 *The enhanced electrocaloric effect in P (VDF-TrFE) copolymer with barium strontium titanate nano-fillers synthesized via an effective hydrothermal method.* RSC advances. **5**(76): p. 61946-61954.

46. Liu, Xiao Qiang, et al., 2013 *Enhanced Electrocaloric Effects in Spark Plasma-Sintered Ba 0.65 Sr 0.35 TiO 3-Based Ceramics at Room Temperature.* Journal of the American Ceramic Society. **96**(4): p. 1021-1023.

47. Bai, Yang, et al., 2011 *The giant electrocaloric effect and high effective cooling power near room temperature for BaTiO3 thick film.* Journal of applied physics. **110**(9): p. 094103.

48. Ye, Hui-Jian, et al., 2014 *Giant electrocaloric effect in BaZr0. 2Ti0. 8O3 thick film.* Applied Physics Letters. **105**(15): p. 152908.

49. Bai, Yang, et al., 2012 *Entropy-change measurement of electrocaloric effect of BaTiO3 single crystal.* physica status solidi (a). **209**(5): p. 941-944.

50. Liu, Shujuan, et al., 2018 *Tunable electrocaloric and energy storage behavior in the Ce, Mn hybrid doped BaTiO3 ceramics.* Journal of the European Ceramic Society. **38**(14): p. 4664-4669.

51. Kandula, Kumara R., et al., 2018 *Enhanced Electrocaloric Effect and Energy Storage Density of Nd-Substituted 0.92 NBT-0.08 BT Lead Free Ceramic.* physica status solidi (a). **215**(7): p. 1700915.

52. Rožič, Brigita, et al., 2011 *Influence of the critical point on the electrocaloric response of relaxor ferroelectrics.* Journal of Applied Physics. **110**(6): p. 064118.

53. Peng, Biaolin, Huiqing Fan, and Qi Zhang, 2013 *A giant electrocaloric effect in nanoscale antiferroelectric and ferroelectric phases coexisting in a relaxor Pb0. 8Ba0. 2ZrO3 thin film at room temperature.* Advanced Functional Materials. **23**(23): p. 2987-2992.

54. Li, Xinyu, et al., 2011 *Tunable temperature dependence of electrocaloric effect in ferroelectric relaxor poly (vinylidene fluoride-trifluoroethylene-chlorofluoroethylene terpolymer.* Applied Physics Letters. **99**(5): p. 052907.

55. Lu, SG, et al., 2010 *Organic and inorganic relaxor ferroelectrics with giant electrocaloric effect.* Applied Physics Letters. **97**(16): p. 162904.

56. Chen, Xiang.-zhong., et al., 2012 *Enhanced electrocaloric effect in poly (vinylidene fluoride-trifluoroethylene)-based terpolymer/copolymer blends.* Applied Physics Letters. **100**(22): p. 222902.

57. Zhang, Guangzu, et al., 2015 *Ferroelectric polymer nanocomposites for room-temperature electrocaloric refrigeration.* Advanced materials. **27**(8): p. 1450-1454.

58. Ma, Rujun, et al., 2017 *Highly efficient electrocaloric cooling with electrostatic actuation.* Science. **357**(6356): p. 1130-1134.

59. Zhang, Tian, et al., 2017 *An electrocaloric refrigerator with direct solid to solid regeneration.* Applied Physics Letters. **110**(24): p. 243503.

60. Zhang, Guangzu, et al., 2018 *Ferroelectric polymer nanocomposites with complementary nanostructured fillers for electrocaloric cooling with high power density and great efficiency.* ACS Applied Energy Materials. **1**(3): p. 1344-1354.

61. Aziguli, Haibibu, et al., 2018 *Enhanced electrocaloric effect in lead-free organic and inorganic relaxor ferroelectric composites near room temperature.* Applied Physics Letters. **112**(19): p. 193902.

62. Qian, Jianfeng, et al., 2019 *Interfacial Coupling Boosts Giant Electrocaloric Effects in Relaxor Polymer Nanocomposites: In Situ Characterization and Phase-Field Simulation.* Advanced Materials. **31**(5): p. 1801949.

63. Lu, Yu.-Chen., et al., 2019 *Enhanced electrocaloric effect for refrigeration in lead-free polymer composite films with an optimal filler loading.* Applied Physics Letters. **114**(23): p. 233901.

64. Wang, Xiangjan, et al., 2015 *Giant electrocaloric effect in lead-free Ba0. 94Ca0. 06Ti1− x Sn x O3 ceramics with tunable Curie temperature.* Applied Physics Letters. **107**(25): p. 252905.

65. Bhalla, Amar S., et al., 2019 *Advances in Ceramics for Environmental, Functional, Structural, and Energy Applications II*. Vol. 266. 2019: John Wiley & Sons, ISBN:1119631483.

66. Schultze, J.W., T. Osaka, and M. Datta, 2002 *Electrochemical microsystem technologies*: CRC Press, ISBN:020321921X.

67. Samitsu, Sadaki, et al., 2013 *Flash freezing route to mesoporous polymer nanofibre networks.* Nature communications. **4**(1): p. 1-7.

68. Elizalde, Cynthia Noemi Baeza, et al., 2018 *Fabrication of blend polyvinylidene fluoride/chitosan membranes for enhanced flux and fouling resistance.* Separation and Purification Technology. **190**: p. 68-76.

69. Stetefeld, Jörg, Sean A. McKenna, and Trushar R. Patel, 2016 *Dynamic light scattering: a practical guide and applications in biomedical sciences.* Biophysical reviews,. **8**(4): p. 409-427.

70. Bhattacharjee, Sourav, 2016 *DLS and zeta potential–what they are and what they are not?* Journal of Controlled Release. **235**: p. 337-351.

71. Honda, Makoto, 1990 *The Impedance measurement Handbook: A guide to measurement technology and techniques*: Hewlett-Packard Company.

72. Zhao, Chunlin, et al., 2016 *Composition-driven phase boundary and electrical properties in (Ba 0.94 Ca 0.06)(Ti 1–x M x) O 3 (M= Sn, Hf, Zr) lead-free ceramics.* Dalton Transactions. **45**(15): p. 6466-6480.

73. Semenov, Alexander, et al., 2019 *Mn-Doped BaTiO3 Ceramics: Thermal and Electrical Properties for Multicaloric Applications.* Materials. **12**(21): p. 3592.

74. Cain, Markys G., 2014 *Characterisation of ferroelectric bulk materials and thin films*. Vol. 2: Springer, ISBN:140209311X.

75. Moya, Xavier, et al., 2013 *Giant electrocaloric strength in single-crystal BaTiO3.* Advanced Materials. **25**(9): p. 1360-1365.

76. Chen, X.iang-Zhong., et al., 2013 *A polymer blend approach to tailor the ferroelectric responses in P (VDF–TrFE) based copolymers.* Polymer. **54**(9): p. 2373-2381.

77. Singh, Pramod K. and MS Gaur, 2018 *Enhancement of β-phase of P (VDF-TrFE) 60/40 by BaTiO3 nanofiller.* Ferroelectrics,. **524**(1): p. 37-43.

78. Li, Zhi-Min, Milind D. Arbatti, and Z.-Y. Cheng, 2004 *Recrystallization study of high-energy electron-irradiated P (VDF− TrFE) 65/35 copolymer.* Macromolecules. **37**(1): p. 79-85.

79. Liu, Yang, et al., 2018 *Ferroelectric polymers exhibiting behaviour reminiscent of a morphotropic phase boundary.* Nature. **562**(7725): p. 96-100.

80. Hu, Xiaoran, et al., 2019 *Wearable piezoelectric nanogenerators based on reduced graphene oxide and in situ polarization-enhanced PVDF-TrFE films.* Journal of materials science. **54**(8): p. 6401-6409.

81. Chang, Shinn-Jen, et al., 2009 *An efficient approach to derive hydroxyl groups on the surface of barium titanate nanoparticles to improve its chemical modification ability.* Journal of Colloid and Interface Science. **329**(2): p. 300-305.

82. Utara, Songkot and Sitchai Hunpratub, 2018 *Effect of BCT-BZT ceramic loading on dielectric properties of natural rubber composites.* Integrated Ferroelectrics. **192**(1): p. 130-140.

83. Jung, Han.-Bo, et al., 2020 *Energy Storage Properties of Blended Polymer Films with Normal Ferroelectric P (VDF-HFP) and Relaxor Ferroelectric P (VDF-TrFE-CFE).* Electronic Materials Letters. **16**(1): p. 47-54.

84. Chen, Jiayung, et al., 2019 *P (VDF-TrFE)/PMMA Blended Films with Enhanced Electrowetting Responses and Superior Energy Storage Performance.* Polymers. **11**(3): p. 526.

85. Tse, Mei.-Yan, et al., 2018 *Enhanced dielectric properties of colossal permittivity co-doped TiO 2/polymer composite films.* RSC advances. **8**(57): p. 32972-32978.

86. Senthil, V., et al., 2012 *Dielectric relaxation behavior and electrical conduction mechanism in polymer-ceramic composites based on Sr modified Barium Zirconium Titanate ceramic.* Journal of Polymer Research. **19**(7): p. 9898.

87. Costa, Carlos M., et al., 2010 *Influence of processing parameters on the polymer phase, microstructure and macroscopic properties of poly (vinilidene fluoride)/Pb (Zr0. 53Ti0. 47) O3 composites.* Journal of non-crystalline solids. **356**(41-42): p. 2127-2133.

88. Arshad, AN, et al., 2019 *Dielectric and Structural Properties of Poly (vinylidene fluoride)(PVDF) and Poly (vinylidene fluoride-trifluoroethylene)(PVDF-TrFE) Filled with Magnesium Oxide Nanofillers.* Journal of Nanomaterials, ISSN: 1687-4110.

89. Li, Qingqink, et al., 2019 *A molecular ferroelectrics induced electroactive β-phase in solution processed PVDF films for flexible piezoelectric sensors.* Journal of Materials Chemistry C. **7**(6): p. 1532-1543.

90. Jiang, Yongchang, et al., 2019 *Enhanced Dielectric Performance of P (VDF-HFP) Composites with Satellite–Core-Structured Fe2O3@ BaTiO3 Nanofillers.* Polymers. **11**(10): p. 1541.

91. Dietze, Matthias and Muhammed Es-Souni, 2019 *Dielectric and pyroelectric properties of thick and thin film relaxor-ceramic/PVDF-TrFE composites.* Functional Composites and Structures. **1**(3): p. 035005.

92. Sebastian, Mailadil T. and Helil Jantunen, 2010 *Polymer–ceramic composites of 0–3 connectivity for circuits in electronics: a review.* International Journal of Applied Ceramic Technology. **7**(4): p. 415-434.

93. Chu, Huiying, et al., 2019 *Enhancing released electrical energy density of poly (vinylidene fluoride-co-trifluoroethylene)-graft-poly (methyl methacrylate) via the pre-irradiation method.* Applied Surface Science. **465**: p. 643-655.

94. Zhang, Lin, et al., 2012 *Dielectric characteristics of CaCu 3 Ti 4 O 12/P (VDF-TrFE) nanocomposites.* Applied Physics A. **107**(3): p. 597-602.

95. Ullah, Amir, et al., 2015 *Enhancement of dielectric and energy density properties in the PVDF-based copolymer/terpolymer blends.* Polymer Engineering & Science,. **55**(6): p. 1396-1402.

96. Liu, ZD., Y. Feng, and WL Li, 2015 *High dielectric constant and low loss of polymeric dielectric composites filled by carbon nanotubes adhering BaTiO 3 hybrid particles.* RSC Advances. **5**(37): p. 29017-29021.

97. Zhang, Yue, et al., 2019 *Excellent energy storage performance and thermal property of polymer-based composite induced by multifunctional one-dimensional nanofibers oriented in-plane direction.* Nano energy. **56**: p. 138-150.

98. Liu, Shaohui, et al., 2016 *Surface-modified Ba (Zr 0.3 Ti 0.7) O 3 nanofibers by polyvinylpyrrolidone filler for poly (vinylidene fluoride) composites with enhanced dielectric constant and energy storage density.* Scientific reports. **6**: p. 26198.

99. Jiang, Zhi-Yuan, et al., 2017 *Exceptionally high negative electro-caloric effects of poly (VDF–co–TrFE) based nanocomposites tuned by the geometries of barium titanate nanofillers.* Polymers. **9**(8): p. 315.

100. Dietze, M., et al., 2007 *Thick film polymer-ceramic composites for pyroelectric applications.* Journal of Applied Physics. **101**(5): p. 054113.

101. Jayasundere, N. and BV Smith, 1993 *Dielectric constant for binary piezoelectric 0-3 composites.* Journal of Applied Physics,. **73**(5): p. 2462-2466.

102. Luo, Bingcheng, et al., 2014 *Fabrication, characterization, properties and theoretical analysis of ceramic/PVDF composite flexible films with high dielectric constant and low dielectric loss.* Journal of Materials Chemistry A. **2**(2): p. 510-519.

103. Silibin, MaximV., et al., 2015 *Polarization reversal in organic-inorganic ferroelectric composites: Modeling and experiment.* Applied Physics Letters. **107**(14): p. 142907.

104. Mahdi, RI, et al., 2015 *Ferroelectric and pyroelectric properties of novel lead-free polyvinylidenefluoride-trifluoroethylene–Bi0. 5Na0. 5TiO3 nanocomposite thin films for sensing applications.* Ceramics International. **41**(10): p. 13836-13843.

105. Belovickis, Jaroslavas, et al., 2018 *Dielectric, Ferroelectric, and Piezoelectric Investigation of Polymer-Based P (VDF-TrFE) Composites.* physica status solidi (b). **255**(3): p. 1700196.

106. CK, Subash, et al., 2015 *Device level optimization of poly (vinylidene fluoride-trifluoroethylene)–zinc oxide polymer nanocomposite thin films for ferroelectric applications.* Journal of Applied Physics. **118**(20): p. 204102.

107. Mahdi, Rahman Ismael, et al., 2018 *Ferroelectric polarization and pyroelectric activity of functionalized P (VDF-TrFE) thin film lead free nanocomposites.* Polymer. **141**: p. 184-193.

108. Feng, Tingting, et al., 2013 *Temperature control of P (VDF-TrFE) copolymer thin films.* Integrated Ferroelectrics. **141**(1): p. 187-194.

109. Liu, Hongbo and X. Yang, 2015 *Theoretical prediction of electrocaloric effect based on non-linear behaviors of dielectric permittivity under temperature and electric fields.* AIP Advances. **5**(11): p. 117134.

110. Handbook-MIL-HDBK, M., *17-1F: Composite Materials Handbook, Volume 1-Polymer Matrix Composites Guidelines for Characterization of Structural Materials.* US Department of Defense, ELECTRONIC ISBN: p. 978-1.

111. Neese, Bret P., 2009 *Investigations of structure-property relationships to enhance the multifunctional properties of PVDF-based polymers.*.

112. Wang, Ru-Min, Shui.-Rong. Zheng, and Yujun George Zheng, 2011 *Polymer matrix composites and technology*: Elsevier.ISBN:085709227.

113. Chen, Xiang.-Zhong, et al., 2013 *A nanocomposite approach to tailor electrocaloric effect in ferroelectric polymer.* Polymer. **54**(20): p. 5299-5302.